NASA Technical Paper 1336

Aerodynamic Derivatives for
an Oblique Wing Aircraft Estimated
From Flight Data by Using
a Maximum Likelihood Technique

Richard E. Maine

NASA

Aerodynamic Derivatives for an Oblique Wing Aircraft Estimated From Flight Data by Using a Maximum Likelihood Technique

Richard E. Maine
Dryden Flight Research Center
Edwards, California

AERODYNAMIC DERIVATIVES FOR AN OBLIQUE WING AIRCRAFT ESTIMATED

FROM FLIGHT DATA BY USING A MAXIMUM LIKELIHOOD TECHNIQUE

Richard E. Maine
Dryden Flight Research Center

INTRODUCTION

The oblique wing configuration is of interest because of its potential for transonic drag reduction and corresponding fuel savings. However, there are several unanswered questions about the aerodynamic characteristics of oblique wing aircraft and the control laws necessary to achieve acceptable handling qualities. Before the oblique wing concept can be developed to its full potential it will be necessary to develop techniques to verify the aerodynamic characteristics of unsymmetrical aircraft in flight.

The theory of estimation of stability and control derivatives (refs. 1 to 5) can be readily applied to oblique wing aircraft by using a five-degree-of-freedom model, but computational complexity and difficulties in maneuver selection make this approach unattractive. This report describes a technique previously used for symmetrical aircraft (ref. 4) that simplifies the estimation by separating the analysis of the longitudinal and lateral-directional motions without neglecting the cross-coupling terms. The technique was briefly described in reference 6.

A flight test program was conducted with a small, remotely piloted, oblique wing aircraft. Maneuvers were performed at wing skew angles of 0° to 45°. The resulting data were digitally filtered and used to estimate a complete set of stability and control derivatives. The derivative estimates obtained are presented and compared to predictions.

SYMBOLS AND ABBREVIATIONS

All data are referenced to fuselage body axes according to right-handed sign conventions.

a_n normal acceleration, g

a_x longitudinal acceleration, g

a_y	lateral acceleration, g
b	reference span, m
b_L, b_N	dummy variables (p. 6)
C_L	nondimensional lift coefficient
C_ℓ	nondimensional rolling-moment coefficient
C_m	nondimensional pitching-moment coefficient
C_N	nondimensional normal-force coefficient
C_n	nondimensional yawing-moment coefficient
C_Y	nondimensional side-force coefficient
c	reference chord, m
$f(\ )$	general function
G	spectral density of measurement noise
g	acceleration due to gravity, m/sec^2
$g(\ )$	general function
I_X	moment of inertia about roll axis, kg-m^2
I_{X_P}	propeller moment of inertia about roll axis, kg-m^2
I_{XY}	cross product of inertia between roll and pitch axes, kg-m^2
I_{XZ}	cross product of inertia between roll and yaw axes, kg-m^2
I_Y	moment of inertia about pitch axis, kg-m^2
I_Z	moment of inertia about yaw axis, kg-m^2
J	cost functional

2

K_L, K_N	dummy variables (p. 6)
K_α	angle of attack upwash factor
M	mass, kg
PCM	pulse code modulation
PSD	power spectral density
p	roll rate, deg/sec or rad/sec
q	pitch rate, deg/sec or rad/sec
$\bar{q}$	dynamic pressure, N/m^2
r	yaw rate, deg/sec or rad/sec
s	reference area, m^2
T	maneuver duration, sec
t	time, sec
u	input vector
V	velocity, m/sec
x	state vector
x_{a_n}, x_{a_y}, x_α, x_β	longitudinal offsets of instruments from center of gravity, m
z	measured observation vector
z	discrete time transfer function variable
z_{a_y}, z_β	vertical offsets of instruments from center of gravity, m
$\hat{z}_\xi$	computed observation vector
α	angle of attack, deg
β	angle of sideslip, deg
Δ	increment

δ_a	aileron deflection (left minus right), deg
δ_e	elevator deflection, deg
δ_r	rudder deflection, deg
η	measurement noise vector
θ	pitch attitude, deg
ξ	vector of unknown coefficients
ρ	air density, kg/m^3
φ	bank angle, deg
ω_p	propeller speed, rad/sec

Superscripts:

m	measured
*	matrix adjoint
•	derivative with respect to time

Subscripts:

c	computed observation
p, q, r, α, β, δ_a, δ_e, δ_r	derivative with respect to indicated quantity
0	bias

VEHICLE AND INSTRUMENTATION

To investigate the feasibility of flying an oblique wing aircraft, the NASA Dryden Flight Research Center and the NASA Ames Research Center have conducted flight tests with a small oblique wing aircraft, which is referred to hereinafter as the oblique wing (fig. 1, ref. 7). The aircraft's wing was capable of being skewed up to 45° left wing forward. The aircraft was flown in two configurations, the short and long tail versions, with lengths of approximately 6.6 and 7.6 meters, respectively (fig. 2). The geometric characteristics of the vehicle are given in table 1. Power was provided by a 90-horsepower, four-cylinder, air-cooled, two-stroke, reciprocating engine that drove a ducted midfuselage three-bladed

propeller with a cruise speed of approximately 3600 rpm. The propeller rotated clockwise viewed from the front of the aircraft. A fixed tricycle landing gear allowed horizontal takeoffs and landings on a dry lakebed.

The aircraft was equipped with an all-movable tail and conventional rudder and aileron surfaces that were controlled remotely by a pilot in a ground cockpit. Telemetry links were used to send pilot control inputs to the vehicle and to return aircraft response data to the ground for the pilot display. In addition, a television camera was mounted in the aircraft's nose, and the picture was displayed in the ground cockpit.

The augmentation system consisted of pitch and roll attitude feedback. Three attempts to utilize the pitch augmentation resulted in dynamic instabilities, so it was not used for the remainder of the program. The roll augmentation was on during several of the test maneuvers, but it had no noticeable effect on the estimates.

The vehicle's weight and center of gravity were measured on balance scales for each wing skew angle. The moments of inertia for the long tail configuration were estimated from swing tests (ref. 8) of the assembled vehicle after the last flight. The moments of inertia for the short tail configuration were estimated by subtracting the predicted differences from the long tail values. The mass data for the short tail configuration are given in table 2. For this configuration, the fuel tank was near enough to the center of gravity and the fuel weight low enough so that the moments of inertia did not change significantly during the data-gathering portion of the flight. For the long tail configuration, a second fuel tank was added near the front of the vehicle. Consequently, the changes in the moments of inertia during the long tail flights were significant. Table 3 gives the long tail mass data as a function of fuel loading.

All the standard stability and control variables were instrumented, including static and total pressures, control surface positions, vehicle attitudes and angular rates, linear accelerations, and angles of attack and sideslip. The angle of attack and sideslip measurements were taken from standard boom-mounted metal vanes, and control surface positions were measured by control position transducers on the control surfaces. Table 4 shows the vane and accelerometer locations. The locations are given relative to the reference center of gravity, which was 0.01 meter above the centerline at 29.3 percent of the reference chord.

The data were sampled at 200 samples per second by an 8-bit pulse code modulation (PCM) system and telemetered to the ground for recording. The resolutions of the PCM signals are listed in table 5.

The angle of attack measurement was unusable for approximately one-third of the second flight. Maneuvers obtained during this period were analyzed without using the angle of attack measurement. No other instrumentation problems were observed.

5

A digital filter was used after the flight to remove the effects of several structural modes that were excited by engine vibration. The filter consisted of both a notch at 17.7 hertz and a third-order Butterworth lowpass with a break frequency of 20 hertz.

The z-plane transfer function of the low pass was

$$K_L \frac{(z + 1)^3}{\left[z^2 - 2e^{-0.866b_L} \cos (0.5b_L)z + e^{-1.732b_L} \right] \left(z - e^{-b_L} \right)}$$

where

$$b_L = 20 \frac{2\pi}{200}$$

and

$$K_L = \frac{\left(1 - 2e^{-0.866b_L} \cos 0.5b_L + e^{-1.732b_L} \right) \left(1 - e^{-b_L} \right)}{8}$$

The notch transfer function was $K_N \dfrac{\left[z^2 - 2 \cos (b_N)z + 1 \right]}{\left(z^2 - 2ze^{-0.707b_N} + e^{-1.414b_N} \right)}$

where

$$b_N = 17.7 \frac{2\pi}{200}$$

and

$$K_N = \frac{\left(1 - 2e^{-0.707b_N} + e^{-1.414b_N} \right)}{\left(2 - 2 \cos b_N \right)}$$

Figure 3 shows power spectral density plots of three representative unfiltered signals. The a_n and p plots exhibit several structural modes between 40 hertz and 80 hertz and one broad mode centered at 17.7 hertz. The strong peak at 60 hertz is from engine vibration. A boom bending mode at about 4.5 hertz is evident in the α signal. The boom mode was not filtered out because its frequency was too

6

low to filter without affecting the aerodynamic modes. The magnitude of the boom oscillation was not large enough to cause problems in the analysis. The power spectral densities of the filtered data are shown in figure 4. The high frequency modes are significantly attenuated. The boom bending mode in the α signal is essentially unaffected, as expected. Time histories of the longitudinal signals are shown before and after filtering in figures 5 and 6, respectively. Marked improvement in a_n and q is apparent in the filtered data with no noticeable phase shift or attenuation in the aerodynamic responses. The boom structural mode can be observed near the end of the filtered α time history.

If the unfiltered data are thinned below 200 samples per second, aliasing of the 40-hertz to 80-hertz structural responses becomes a problem. In the thinned data, these responses are folded down to lower frequencies and cannot be separated from the rigid body response. The folding is illustrated by figure 7, which is the power spectral density of the unfiltered a_n thinned to 25 samples per second. The structural modes from figure 3 have folded down and spread over the spectrum between 0 hertz and 12.5 hertz, with the result that the spectrum is nearly white. It would be almost impossible to recover a good signal from these data; therefore, 200-sample-per-second data were necessary for filtering out the structural response. After filtering, the data were thinned to 25 samples per second for analysis.

FLIGHT TEST PROCEDURE

The flight program was limited to three flights of approximately 1 hour each. Longitudinal stability problems required a configuration change after the first flight (the tail was moved back 1 m), leaving only two flights in the final configuration. Since the flights were separated by only a few weeks, only a preliminary data analysis could be performed between flights. Thus no time was available to experiment with different maneuvers for the identification of the stability and control derivatives.

The pilot performed 87 maneuvers for stability and control data during the three flights. Elevator doublets were used for longitudinal maneuvers; each lateral-directional maneuver included a rudder doublet and an aileron doublet. The instability in the pitch augmentation system caused three unplanned elevator oscillations in the first flight which were also used as test maneuvers. Radio interference problems resulted in several periods of apparently random control surface motion, seven of which were selected as test maneuvers for analysis. Analysis was attempted on these 97 maneuvers, some of which involved inputs to both the longitudinal and lateral-directional control surfaces.

The phugoid mode was relatively difficult to control because of the small size and low speed of the vehicle; thus, many of the maneuvers were obtained when flight conditions were not well stabilized. The phugoid problem was worse when the quality of the television picture was poor, since the pilot depended heavily on television for attitude reference. The radio interference problems mentioned above also increased the pilot's workload considerably.

PREDICTED AERODYNAMIC CHARACTERISTICS

Predictions of the static derivatives were based on data obtained from full-scale tests conducted in the Ames 40- by 80-Foot Wind Tunnel. The actual flight vehicle in the short tail configuration was placed in the wind tunnel to obtain the data. Rotary damping derivatives were predicted theoretically by using lifting line theory (ref. 9). Predictions for the long tail configuration were obtained empirically by multiplying the short tail predictions of C_{m_α}, C_{n_β}, $C_{m_{\delta_e}}$, and $C_{n_{\delta_r}}$ by 1.33 (the ratio of the tail volumes); for C_{m_q} and C_{n_r} a ratio of 1.77 (1.33^2) was used.

The wind tunnel data presented herein are corrected for power effects and are referenced to a center of gravity of 29.3 percent of the reference chord.

The vehicle was tested in the wind tunnel in both the short and the long tail configurations. There was a significant difference between the wind tunnel and flight test versions of the aircraft. The difference concerned the tail boom and the truss arrangement that attached the empennage to the vehicle. For the wind tunnel tests, the tail boom was composed of several interchangeable parts to facilitate the testing of various tail lengths. This caused considerably more tail boom flexibility than in the flight vehicle, in which the tail boom was a solid tube and quite rigid. The flexibility of the wind tunnel vehicle in the long tail configuration was great enough so that the long tail data were judged unusable. Therefore, the simple empirical factors mentioned above were used to obtain predicted long tail derivatives from the short tail predictions. The flexibility of the wind tunnel vehicle in the short tail configuration was not as extreme, but it still opens the validity of the predictions to question.

Analysis of the static data was further complicated by the fairly large scatter in some of the data. The scatter was due in part to the aircraft's size, which was small for the wind tunnel's data acquisition system. For example, over the range of angle of attack for which flight data are presented ($3°$ to $9°$), the aircraft's pitching-moment coefficient increment is approximately -0.0400 on the basis of the static wind tunnel data. This value is only three times or so as large as the quoted resolution of each static data point in the range. The scatter was great enough so that C_{m_α} predictions could vary by a factor of 2 or 3 for the same flight condition and configuration, depending on the fairing used and the breakpoints plotted. The wind tunnel rolling-moment derivatives also exhibited a large amount of scatter, and in some cases the scatter made the predicted roll-related coefficients questionable.

METHOD OF ANALYSIS

The maximum likelihood estimation method was used to analyze the oblique wing data. This method is widely accepted as one of the best techniques for

estimating stability and control derivatives from flight data. The maximum likelihood method for systems with measurement noise but no state noise is briefly reviewed below. Further discussion is to be found in reference 2.

The system is defined by the following equations:

$$\dot{x}(t) = f[x(t), u(t), \xi]$$

$$z(t) = g[x(t), u(t), \xi] + \eta(t)$$

where

x	state vector
u	input vector
ξ	vector of unknown coefficients
z	measured observation vector
η	measurement noise vector

If η is assumed to be band limited, white, zero mean, Gaussian noise with spectral density G, the maximum likelihood estimate is obtained by choosing ξ to minimize the cost functional

$$J(\xi) = \int_0^T \left[\hat{z}_\xi(t) - z(t) \right]^* (GG^*)^{-1} \left[\hat{z}_\xi(t) - z(t) \right] dt$$

where $\hat{z}_\xi$ is the observation vector obtained by integrating the system equations with the assumed value of ξ and no noise. An extra term is often included in maximum likelihood estimation routines to include the effects of *a priori* information, but this feature was not used for the analysis described in this paper.

A modified Newton-Raphson (Newton-Balakrishnan) iterative algorithm is used to minimize J (refs. 2 and 3).

Five-Degree-of-Freedom Approach

The five-degree-of-freedom approach to the analysis of oblique wing data is the most straightforward approach, and it is suggested by many investigators. However, because of the difficulties inherent in the five-degree-of-freedom approach, it was not used on the oblique wing data; instead, a simpler approach was sought.

It is generally accepted that five-degree-of-freedom equations of motion are necessary for the analysis of oblique wing data (the sixth degree of freedom, velocity, can still be ignored). Three types of coupling between the longitudinal and lateral-directional motions combine to invalidate the standard three-degree-of-freedom assumptions. The kinematic coupling terms present but often ignored for symmetrical aircraft are larger for the oblique wing, because for the oblique wing, significant

motion is present in all axes. Kinematic coupling terms not present for symmetrical aircraft arise because of the nonzero I_{XY} of the oblique wing. Finally, the oblique wing results in significant aerodynamic coupling between the modes.

The application of the maximum likelihood estimation method to the five-degree-of-freedom equations for the oblique wing is straightforward from a theoretical standpoint; however, problems abound in the practical application of the technique. There are seven states, nine observations, and three controls. With the derivatives we choose to estimate there would be 39 unknowns, so computation time would be relatively long. Some numerical problems are also to be expected from handling equations with 39 unknowns. Although this number of unknowns is not large enough to make the problems extreme, double precision would almost surely be required if a 32-bit computer were used; naturally, double precision would not help the computation time problem.

Maneuvers must be carefully selected and performed to excite the modes enough to permit an accurate simultaneous estimation of all the coefficients. The selection and refinement of the maneuvers would be particularly difficult in a short flight program such as that for the oblique wing.

Overall, it was judged that it would be difficult to obtain estimates of high quality with the five-degree-of-freedom approach. The inaccuracy of the linear aerodynamic model, the brevity of the flight program, and the difficulties of the five-degree-of-freedom approach combined to make such an analysis a major effort. Therefore, a simpler technique was sought, and the five-degree-of-freedom approach was not used on the oblique wing data.

Analysis by Separation of Modes

Many of the problems arising from the five-degree-of-freedom approach could be alleviated if the longitudinal and lateral-directional motions could be analyzed separately. For conventional aircraft, the motions are usually separated by simply neglecting the cross-coupling terms. For an oblique wing, these terms are too large to neglect.

However, for this aircraft, it is possible to include the effect of the cross-coupling terms without using all five degrees of freedom. This is done in the longitudinal analysis by eliminating the differential equations for the lateral-directional motion and using the measured lateral-directional responses as inputs to the longitudinal equations. Similarly, the lateral-directional analysis uses the measured longitudinal responses.

The longitudinal equations of motion for the oblique wing, including propeller gyroscopic effects, then become

$$\dot{\alpha} = -\frac{\bar{q}s}{MV}C_L + q + \frac{g}{V}\left(\cos\theta\cos\varphi^m\cos\alpha + \sin\theta\sin\alpha\right) - \tan\beta^m\left(p^m\cos\alpha + r^m\sin\alpha\right)$$

$$\dot{q}I_Y - \dot{p}^mI_{XY} = \bar{q}scC_m + r^mp^m(I_Z - I_X) + \left[(r^m)^2 - (p^m)^2\right]I_{XZ} + qr^mI_{XY} + r^m\omega_pI_{X_p}$$

$$\dot{\theta} = q\cos\varphi^m - r^m\sin\varphi^m$$

10

The longitudinal aerodynamic parameters chosen to be estimated for the oblique wing are contained in the following expansions of the nondimensional moments and forces. The reasons for this choice are explained in the section entitled Results and Discussion.

$$C_L = C_{L_\alpha} \alpha + C_{L_{\delta_e}} \delta_e + C_{L_0} + C_{L_\beta} \beta^m$$

$$C_m = C_{m_\alpha} \alpha + C_{m_q} \frac{qc}{2V} + C_{m_{\delta_e}} \delta_e + C_{m_0} + C_{m_{\delta_a}} \delta_a + C_{m_p} \frac{p^m b}{2V} + C_{m_r} \frac{r^m b}{2V} + C_{m_\beta} \beta^m \tag{1}$$

The longitudinal observation equations are:

$$\alpha_c = K_\alpha \left(\alpha - \frac{x_\alpha}{V} q \right)$$

$$q_c = q$$

$$\theta_c = \theta$$

$$a_{n_c} = \frac{\bar{q} s}{Mg} C_N + \frac{x_{a_n}}{g} \dot{q} + a_{n_0}$$

It should be noted that although the $\dot{\alpha}$ equation above contains C_L (lift) derivatives, this report presents C_N (normal-force) derivatives because the sixth degree of freedom, velocity, is not included. For the low angles of attack investigated, this substitution should not cause problems.

The lateral-directional equations are as follows:

$$\dot{\beta} = \frac{\bar{q} s}{MV} C_Y + \frac{g}{V} \cos \theta^m \sin \varphi + p \sin \alpha^m - r \cos \alpha^m$$

$$\dot{p} I_X - \dot{r} I_{XZ} - \dot{q}^m I_{XY} = \bar{q} s b C_\ell + q^m r (I_Y - I_Z) + q^m p I_{XZ} - rp I_{XY}$$

$$\dot{r} I_Z - \dot{p} I_{XZ} = \bar{q} s b C_n + q^m p (I_X - I_Y) - q^m r I_{XZ} + \left[p^2 - (q^m)^2 \right] I_{XY} - q^m \omega_p I_{X_P}$$

$$\dot{\varphi} = p + r \cos \varphi \tan \theta^m + q^m \sin \varphi \tan \theta^m$$

11

where the following coefficient expansions contain the lateral-directional aero-dynamic parameters chosen to be estimated.

$$C_Y = C_{Y_\beta}\beta + C_{Y_{\delta_a}}\delta_a + C_{Y_{\delta_r}}\delta_r + C_{Y_0} + C_{Y_\alpha}\alpha^m$$

$$C_\ell = C_{\ell_\beta}\beta + C_{\ell_p}\frac{pb}{2V} + C_{\ell_r}\frac{rb}{2V} + C_{\ell_{\delta_a}}\delta_a + C_{\ell_{\delta_r}}\delta_r + C_{\ell_0} + C_{\ell_q}\frac{q^m c}{2V} + C_{\ell_\alpha}\alpha^m \qquad \left.\right\} \quad (2)$$

$$C_n = C_{n_\beta}\beta + C_{n_p}\frac{pb}{2V} + C_{n_r}\frac{rb}{2V} + C_{n_{\delta_a}}\delta_a + C_{n_{\delta_r}}\delta_r + C_{n_0} + C_{n_q}\frac{q^m c}{2V} + C_{n_\alpha}\alpha^m$$

The lateral-directional observation equations are:

$$\beta_c = \beta - \frac{z_\beta}{V}p + \frac{x_\beta}{V}r$$

$$p_c = p$$

$$r_c = r$$

$$\varphi_c = \varphi$$

$$a_{y_c} = \frac{\bar{q}s}{Mg}C_Y - \frac{z_{a_y}}{g}\dot{p} + \frac{x_{a_y}}{g}\dot{r} + a_{y_0}$$

In the equations above, the m superscripts denote measured quantities. Both the longitudinal and lateral-directional equations assume small angles of sideslip.

Two assumptions are necessary for this approach. The most important assumption is that measurements of all of the state variables of the unmodeled modes are available and contain relatively low levels of noise contamination. The second assumption is that the magnitudes of the cross-coupling terms are small compared with the standard terms. The second assumption ensures that the errors in the cross-coupling terms caused by using the noise-contaminated measurements do not significantly affect the analysis. Obviously, there is a tradeoff between these two assumptions: The lower the measurement noise, the larger the allowable magnitude of the coupling terms.

This separation technique has previously been used to account for kinematic coupling in the symmetrical aircraft (ref. 4); however, the assumptions inherent in the technique have not been carefully documented. Examination of the assump-

tions shows that the application of the separation technique to the oblique wing requires much more caution than the application of the technique to symmetrical aircraft because of the increased magnitude of the cross-coupling terms. The allowable magnitude of the measurement noise is, therefore, much smaller for the oblique wing.

A slight extension of this separation technique which allows the system to be represented in a linearized manner is accomplished by using measured data from both the longitudinal and lateral-directional modes in the nonlinear terms. The data presented in this report were obtained from equations linearized in this manner by using the following specific procedure. The nonlinear terms were simply computed by using measured data, with two exceptions. The cos θ in the α

equation was replaced by $\cos \theta^m - (\theta - \theta^m) \sin \theta^m$ and the sin φ in the β equation

was replaced by $\sin \varphi^m + (\varphi - \varphi^m) \cos \varphi^m$. This significantly reduces the computer time required. It also allows a standard linear program to be used for the derivative estimation.

The computer program used, MMLE 3, is an outgrowth of the MMLE program (ref. 3). The MMLE 3 program was not written with the oblique wing application in mind, but rather to provide a standard identification program with a general set of linear equations.

It should be possible to incorporate the separation technique proposed into any reasonably general maximum likelihood estimation program.

RESULTS AND DISCUSSION

Coupling between the longitudinal and lateral-directional modes was significant on the oblique wing, as expected. Figure 8 shows a typical time history of the aircraft's response to an elevator input; motion in all of the modes is considerable because of the coupling. Similarly, figure 9 shows that the aircraft responds in both the longitudinal and lateral-directional modes to a maneuver involving rudder and aileron doublets.

The data were analyzed first by ignoring all of the coupling terms. The values used for the G matrix are given in table 6. Although this produced reasonable results for most of the maneuvers at the lower wing skew angles, it was clearly unacceptable in several cases, particularly for those at 30° and 45° of wing skew. One of the unacceptable fits is shown in figure 10.

Then the separation technique was used to include cross-coupling effects in the analysis. The G matrix values given in table 6 were also used for this analysis. Since aerodynamic, as well as kinematic, coupling was significant, it was first

13

necessary to choose the set of derivatives to include in the model. Considerable effort was expended in making this choice. For the final analysis, the derivatives in equations (1) and (2) were chosen. Analysis was started with kinematic coupling only, and derivatives were added to the model one at a time to evaluate their effects. The choice of derivatives was based on physical reasoning, the size of the predicted effects, and the improvement observed in the analysis when each derivative was added to the model.

With these aerodynamic terms included, all 97 maneuvers obtained were successfully analyzed. This 100-percent utilization was quite unexpected for this unconventional aircraft. Figure 11 shows a resulting lateral-directional fit. The fit is good compared with figure 10, which is the fit of the same maneuver with the cross-coupling terms omitted. Figure 12 shows a longitudinal fit, which is excellent.

The final derivative estimates are presented in figures 13 to 20. The vertical bars in these figures are uncertainty levels (refs. 4 and 5), which indicate the approximate accuracy that can be expected of the estimates. The flight estimates in these figures are plotted against an angle of attack adjusted for upwash by dividing the average measured angle of attack for each maneuver by a factor of 1.25. This factor was obtained by averaging the upwash factors estimated for all of the longitudinal maneuvers.

The estimate of the upwash factor for each maneuver was obtained by treating it as one of the unknown parameters for each longitudinal maneuver. No flight estimate of the bias in the angle of attack was available.

The derivative $C_{m_{\dot{\alpha}}}$ is assumed to be zero in the flight estimation model; thus, the flight-estimated C_{m_q} includes the effect of any actual $C_{m_{\dot{\alpha}}}$. The predicted values of $C_{m_q} + C_{m_{\dot{\alpha}}}$ are, therefore, used to compare with flight-estimated C_{m_q} in this report. Similarly, the predicted $C_{m_\alpha} - \frac{\rho s c}{4M} C_{L_\alpha} C_{m_{\dot{\alpha}}}$ is used for comparison with the flight-estimated C_{m_α}. For simplicity, the correction to the predicted C_{m_α} was made by using a nominal mass of 400 kilograms and an air density of 1.104 kg/m^3, which corresponds to a density altitude of 1067 meters.

Short Tail Derivatives

Figure 13 shows the estimates of the lateral-directional derivatives for the short tail configuration. Flight data in this configuration were obtained at 0° and 15° of wing skew angle. The estimates are in reasonably good agreement with predictions, with the notable exception of the rudder derivatives. The flight estimates of

14

$C_{n_{\delta_r}}$ are considerably larger in magnitude than the wind tunnel estimates. The flight data also show an increase in rudder effectiveness as angle of attack increases; this trend is not present in the wind tunnel data. The same discrepancies can be observed in $C_{Y_{\delta_r}}$, although the wind tunnel estimates lie within the uncertainty envelope. The tail flexibility during the wind tunnel tests may account for some of these discrepancies. The flight estimates of $C_{\ell_{\delta_r}}$ are opposite in sign from the wind tunnel estimates. It would be natural to expect a positive value of $C_{\ell_{\delta_r}}$ for a rudder above the fuselage; this is in agreement with the flight estimates. The sign conventions used for the wind tunnel data were checked for consistency with those used for this report, but no discrepancy was found.

Since the short tail flight data were obtained only at wing skew angles of 0° and 15°, the effects of skew angle were not large. The effects of skew, which can be discerned in C_{ℓ_p} and $C_{\ell_{\delta_a}}$, are in excellent agreement with the predicted effects of skew on these derivatives.

The lateral-directional cross-coupling derivatives due to longitudinal motion are presented for the short tail configuration in figure 14. The flight estimates of C_{n_q} are considerably larger in magnitude than predicted, although C_{ℓ_q} is smaller than predicted. The flight estimates of C_{ℓ_q} and C_{n_q} may be partially compensating for a modeling error. The angle of attack derivatives are in good agreement with predictions; the large apparent scatter in C_{ℓ_α} is due to its small magnitude for 0° and 15° of wing skew.

Figure 15 summarizes the short tail longitudinal derivatives. The estimates of C_{N_α} are slightly larger than predicted. The C_{m_α} estimates are in good agreement with the wind tunnel fairing presented here, although, as discussed above, the predicted values of C_{m_α} varied widely.

The flight estimates of $C_{m_{\delta_e}}$ are larger in magnitude than predicted, perhaps because of the tail flexibility during the wind tunnel tests. The larger than predicted elevator effectiveness was a major contributor to a longitudinal sensitivity problem that almost caused the aircraft to crash during the first flight. The flight estimates of C_{m_q} are somewhat larger in magnitude than the predictions.

Figure 16 presents the short tail data for the longitudinal cross-coupling derivatives due to lateral-directional motion. The agreement with predictions is good for all of these derivatives.

Preliminary derivative estimates were obtained approximately 2 weeks after the first flight. These estimates were used to verify the source of the longitudinal sensitivity problem and to update the flight simulator. The pilot commented that the simulator flew much more like the aircraft after being updated. The consistent trends in the final short tail estimates, their low uncertainty levels, and the good fits all indicate that the estimates obtained are reasonably good. The simulator experience provides additional verification of the quality of the estimates.

Long Tail Derivatives

Figure 17 shows the long tail estimates for the lateral-directional derivatives. Long tail flight data were gathered at wing skew angles up to 45°; thus, the skew effects were more easily observed than in the short tail data. The derivative C_{n_β} becomes slightly smaller and C_{ℓ_β} more negative as the wing skew angle increases. The derivatives C_{ℓ_p} and C_{ℓ_r} are smaller in magnitude at the larger skew angles, as expected. No definite effect of skew angle is apparent in C_{n_p} or C_{n_r}. The derivative $C_{\ell_{\delta_a}}$ agrees well with the predictions, decreasing at the larger skew angles. The $C_{n_{\delta_a}}$ estimates at 0° and 15° of wing skew average about 0.0001 for the long tail flight data, as opposed to 0 for the short tail flight data. This difference is almost surely due to a slight error in the estimated inertias for one or both configurations. It is difficult to imagine a significant effect of tail position on the actual $C_{n_{\delta_a}}$; on the other hand, the $C_{n_{\delta_a}}$ estimate from flight data is very sensitive to I_{XZ} (for any estimation technique). The flight $C_{n_{\delta_a}}$ from the long tail data shows a peak at 30° of wing skew, in agreement with predicted trends, although the magnitudes of the flight and predicted values are somewhat different. The rudder derivatives show the same disagreement with predictions as was noted in the short tail data. In addition, the long tail data show that rudder effectiveness decreases as wing skew angle increases.

Figure 18 gives the long tail lateral-directional cross-coupling derivatives due to longitudinal motion. As in the short tail data, the agreement with predictions is poor for the q derivatives and good for the α derivatives.

The estimates of the longitudinal derivatives for the long tail configuration are presented in figure 19. Both C_{N_α} and C_{m_α} become smaller in magnitude as

wing skew angle increases. The disagreement of the flight and wind tunnel estimates of C_{m_α} is not surprising, considering the resolution problems with the wind tunnel test data for the estimation of C_{m_α}. In addition, the factor used to get long tail predicted values from the short tail values (1.33) is not very accurate when applied to C_{m_α}; it neglects the change in downwash and the wing pitching moment. As in the short tail data, $C_{m_{\delta_e}}$ and C_{m_q} are larger in magnitude than predicted. The C_{m_q} estimates are more negative at the larger skew angles.

Figure 20 shows the long tail longitudinal cross-coupling derivatives due to lateral-directional motion. The estimates of C_{m_p}, C_{N_β}, and $C_{m_{\delta_a}}$ are in good agreement with predictions. The derivative C_{m_β} is less negative than predicted. The uncertainty levels and scatter of C_{m_r} are fairly large, although at least its sign seems well established. This indicates that C_{m_r} is probably the weakest of the cross-coupling derivatives estimated.

The trends of the short tail estimates were substantiated by the long tail data. In addition, the long tail data included maneuvers at up to 45° of wing skew angle. As a result, several trends were evident in the long tail estimates that were not observed in the short tail data.

CONCLUDING REMARKS

A technique was described that estimates aircraft aerodynamic derivatives by separating the analysis of longitudinal and lateral-directional motion even in the presence of the moderate cross coupling characteristic of oblique wing aircraft. The technique has several advantages over the usual five-degree-of-freedom approach for some situations. Although previously applied to symmetrical aircraft, this technique was not expected to be adequate for oblique wing vehicles.

This separation technique was applied to obtain a complete set of stability and control derivative estimates from flight data for a small remotely piloted oblique wing aircraft. This application represents the first time that aerodynamic derivatives have been estimated from flight data for such aircraft. Aliasing problems necessitated a 200-sample-per-second rate for the raw data, even though a 25-sample-per-second rate for the filtered data was sufficient for the analysis. The complete set of flight-determined estimates was presented and compared to predictions. Comparisons with predictions were generally reasonable, with some exceptions. The limited number of flights available and the lack of usable wind tunnel data for one of the aircraft

17

configurations prevented the comparison from being definitive. However, the results demonstrated that the relatively simple approach developed was adequate to obtain usable estimates of the aerodynamic derivatives of oblique wing aircraft.

Dryden Flight Research Center
  National Aeronautics and Space Administration
    Edwards, Calif., December 6, 1977

REFERENCES

1. Balakrishnan, A. V.: Stochastic Differential Systems I. Filtering and Control— A Function Space Approach. Lecture Notes in Economics and Mathematical Systems, 84, M. Beckmann, G. Goos, and H. P. Kunzi, eds., Springer-Verlag (Berlin), 1973.

2. Iliff, Kenneth W.; and Taylor, Lawrence W., Jr.: Determination of Stability Derivatives From Flight Data Using a Newton-Raphson Minimization Technique. NASA TN D-6579, 1972.

3. Maine, Richard E.; and Iliff, Kenneth W.: A FORTRAN Program for Determining Aircraft Stability and Control Derivatives From Flight Data. NASA TN D-7831, 1975.

4. Iliff, Kenneth W.; and Maine, Richard E.: Practical Aspects of Using a Maximum Likelihood Estimation Method To Extract Stability and Control Derivatives From Flight Data. NASA TN D-8209, 1976.

5. Iliff, Kenneth W.; and Maine, Richard E.: Further Observations on Maximum Likelihood Estimates of Stability and Control Characteristics Obtained From Flight Data. A Collection of Technical Papers—AIAA Atmospheric Flight Mechanics Conference, AIAA Paper 77-1133, c.1977, pp. 100-112.

6. Maine, Richard E.: Maximum Likelihood Estimation of Aerodynamic Derivatives for an Oblique Wing Aircraft From Flight Data. A Collection of Technical Papers—AIAA Atmospheric Flight Mechanics Conference, AIAA Paper 77-1135, c.1977, pp. 124-133.

7. Bailey, Rodney O.; and Putnam, Peter A.: Oblique Wing, Remotely Piloted Research Aircraft. RPV's: Issues and Perspectives. Proceedings of the Second Annual Symposium of the Nat. Assn. for Remotely Piloted Vehicles, 1975, pp. 25-1—25-17.

8. Wolowicz, Chester H.; and Yancey, Roxanah B.: Experimental Determination of Airplane Mass and Inertial Characteristics. NASA TR R-433, 1974.

9. Fantino, R. E.; Parsons, E. K.; Powell, J. D.; and Shevell, R. S.: Effects of Asymmetry on the Dynamic Stability of Aircraft. NASA CR-142857, 1975.

18

TABLE 1.—GEOMETRIC CHARACTERISTICS OF OBLIQUE WING

Reference area, m^2	9.27
Reference (root) chord, m	1.73
Reference span, m	6.81
Horizontal stabilizer, m—	
Span	2.68
Root chord	0.686
Vertical tail, m—	
Span	0.65
Root chord	0.94
Tip chord	0.40
Rudder span, m	0.45
Aileron span, m	1.83
Propeller diameter, m	1.23
Reference center of gravity—	
Percent of reference chord	29.3
Distance behind nose tip, m	2.286
Vertical center of gravity,	
distance above centerline, m	0.010 (±0.005)

TABLE 2.—MASS DATA FOR OBLIQUE WING SHORT TAIL CONFIGURATION

[Full fuel condition]

(a) Constant data

Mass, kg	388
Center of gravity,	
percent of reference chord	29.3
I_{X_P}, kg-m^2	0.241

(b) Data dependent on wing skew angle

	Wing skew angle, deg	
	0	15
I_X, kg-m^2	314	302
I_Y, kg-m^2	488	510
I_Z, kg-m^2	698	698
I_{XZ}, kg-m^2	69	69
I_{XY}, kg-m^2	0	-54

19

TABLE 3.—MASS DATA FOR OBLIQUE WING LONG TAIL CONFIGURATION

(a) Empty weight data

	Wing skew angle, deg			
	0	15	30	45
I_X, kg-m^2	314	302	262	211
I_Y, kg-m^2	602	622	648	718
I_Z, kg-m^2	824	824	824	824
I_{XZ}, kg-m^2	69	69	69	69
I_{XY}, kg-m^2	0	-54	-94	-108
I_{X_P}, kg-m^2	0.241	0.241	0.241	0.241

(b) Fuel loading data

Time, min	Event	[a]Total mass, kg	Center of gravity, percent c	[b]ΔI_Y and ΔI_{XZ}, kg-m^2	[b]ΔI_{XZ}, kg-m^2
0	Start of takeoff roll	414	28.0	54	3
36	Forward fuel expended	400	31.5	12	3
78	All fuel expended	383	33.2	3	0

[a]Assumes a fuel flow rate of 0.39 kg/min.

[b]The values in these columns are added to the empty weight data
in table 3(a) to obtain the data adjusted for fuel loading.

TABLE 4.—INSTRUMENT LOCATIONS RELATIVE TO REFERENCE CENTER OF GRAVITY

Measured quantity	Distance of instrument forward of reference center of gravity, m	Distance of instrument below reference center of gravity, m
α	2.819	------
β	2.730	0.305
a_n . . .	0.584	------
a_x . . .	-----	-0.098
a_y . . .	0.651	-0.098

TABLE 5.—PCM SIGNAL RESOLUTIONS FOR OBLIQUE WING DATA

Signal	Resolution
α, deg	0.15
β, deg	0.15
p, deg/sec	0.4
q, deg/sec	0.4
r, deg/sec	0.2
θ, deg	0.6
φ, deg	0.7
a_n, g	0.02
a_x, g	0.01
a_y, g	0.01
δ_a, deg	0.1
δ_e, deg	0.1
δ_r, deg	0.15
V, m/sec	0.25
Altitude, m	10

TABLE 6.—G MATRIX VALUES USED IN ANALYZING OBLIQUE WING DATA.

Signal	[a]Diagonal element of G^{-1}
α, per deg	40
q, per deg/sec	24
θ, per deg	34
a_n, per g	380
β, per deg	20
p, per deg/sec	12
r, per deg/sec	15
φ, per deg	13
a_y, per g	650

[a]Off-diagonal elements are all 0.
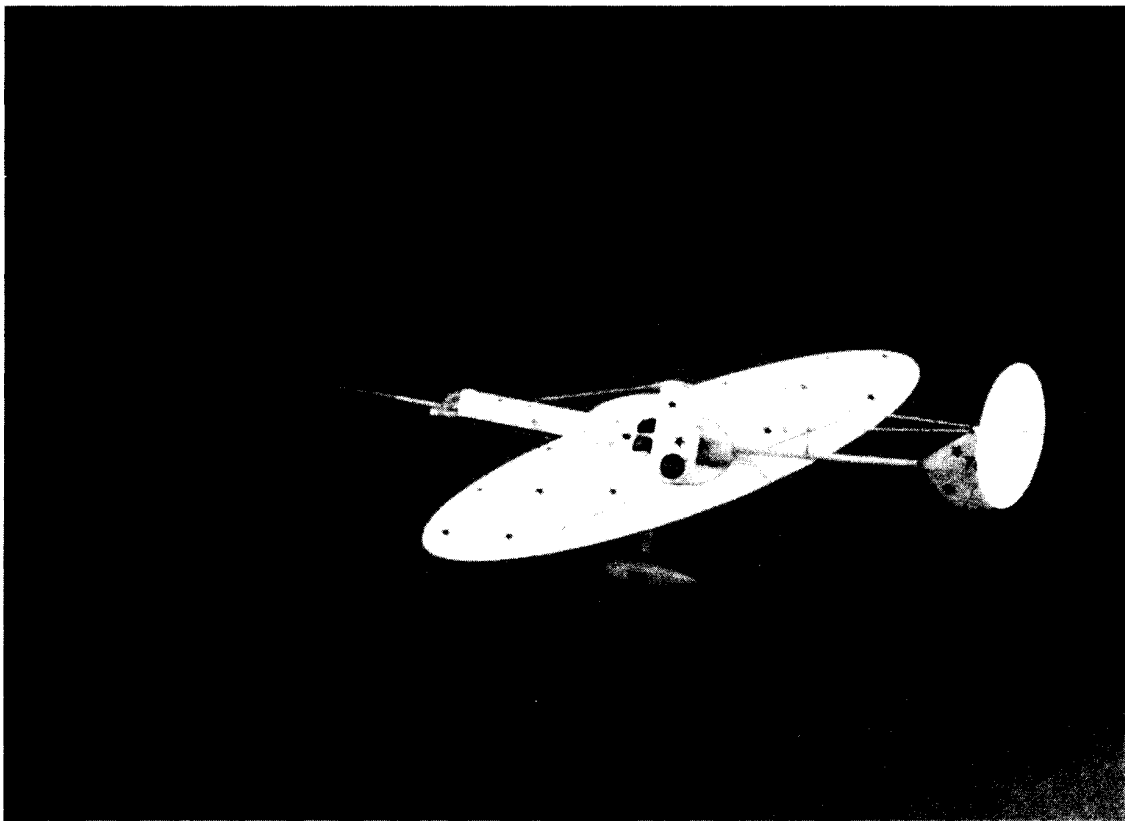
Figure 1. Oblique wing.
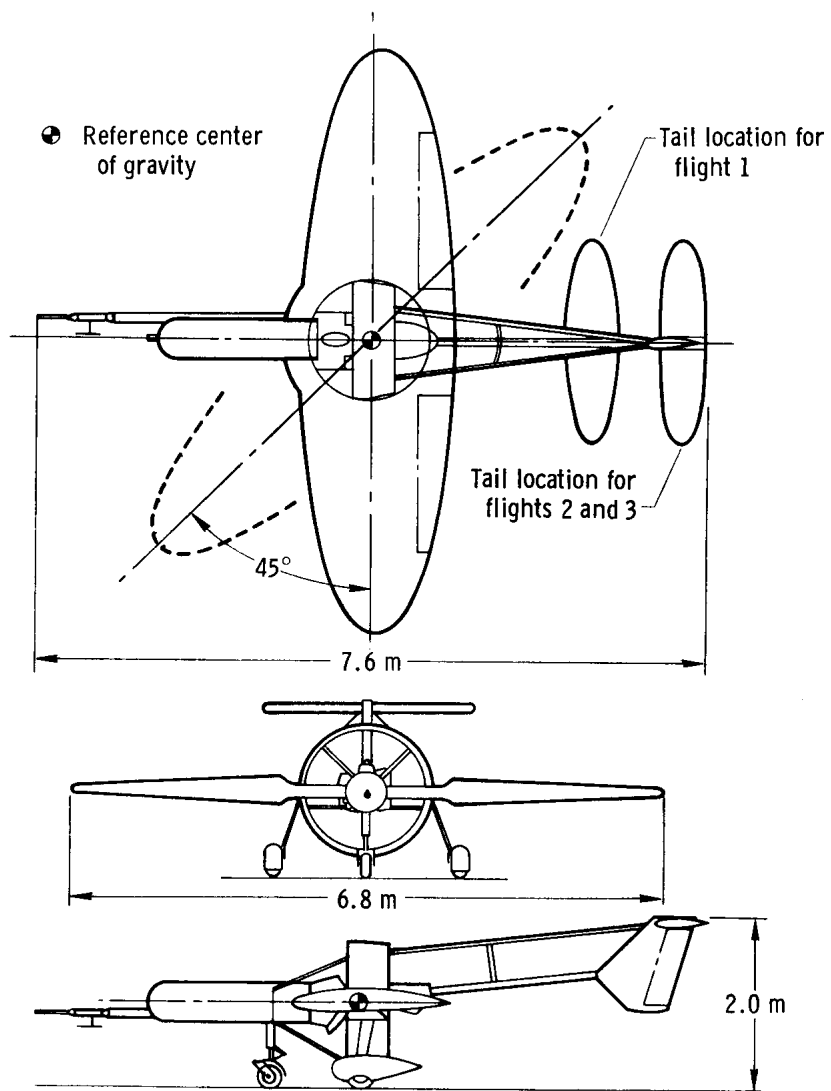
Figure 2. Three-view drawing of oblique wing.
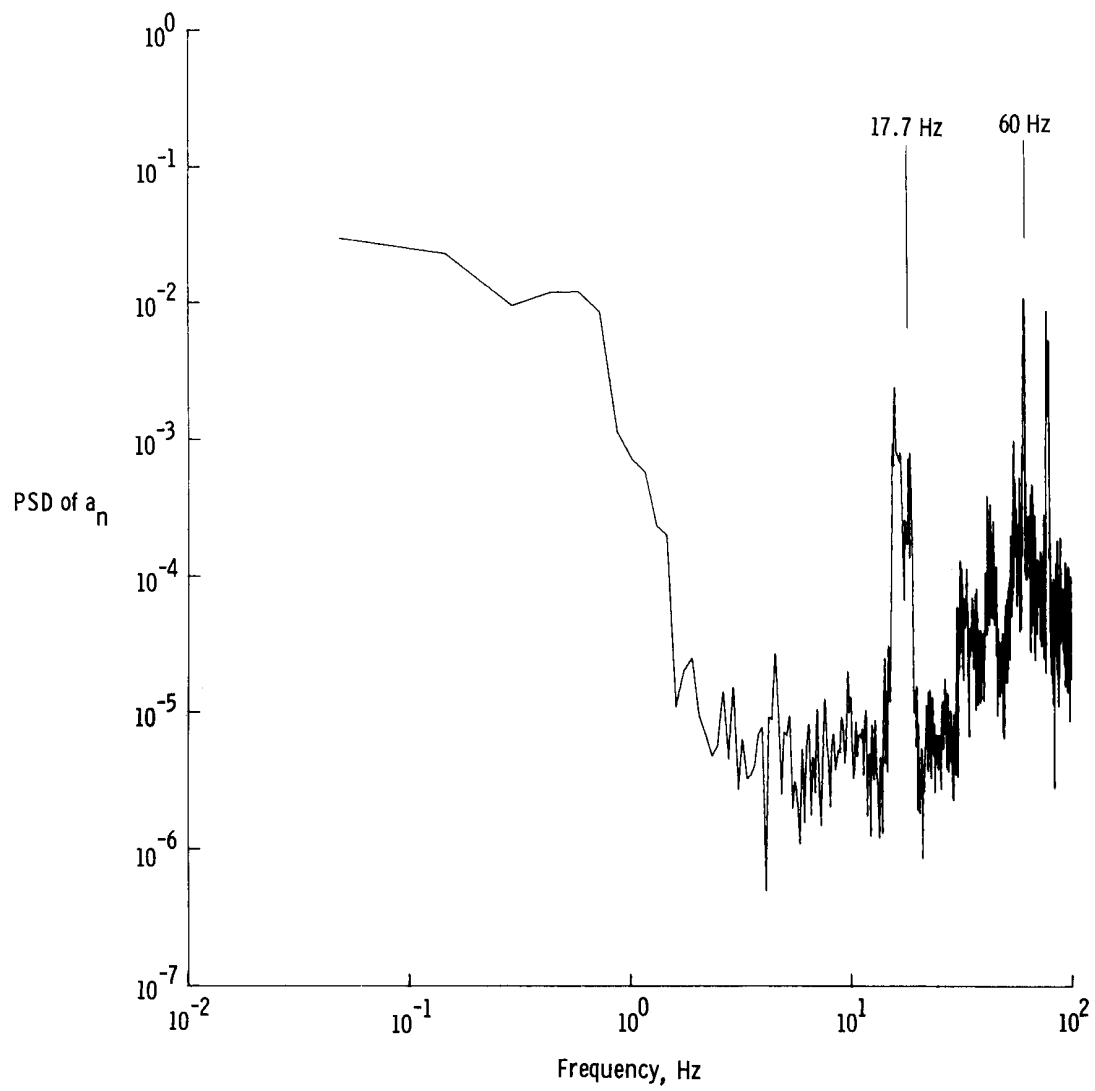
Figure 3. Power spectral densities of unfiltered 200-sample-per-second data.
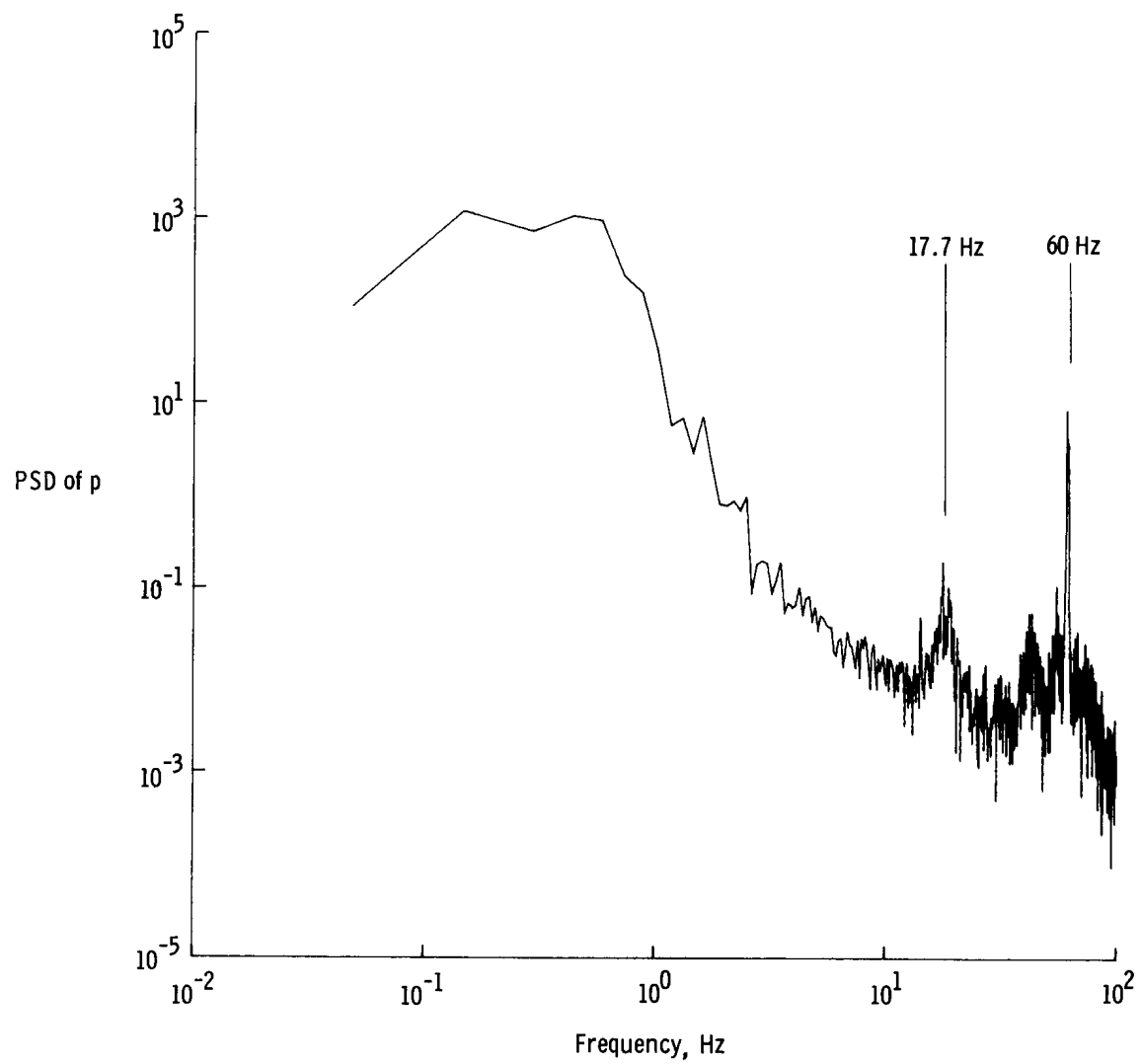
Figure 3. Continued.
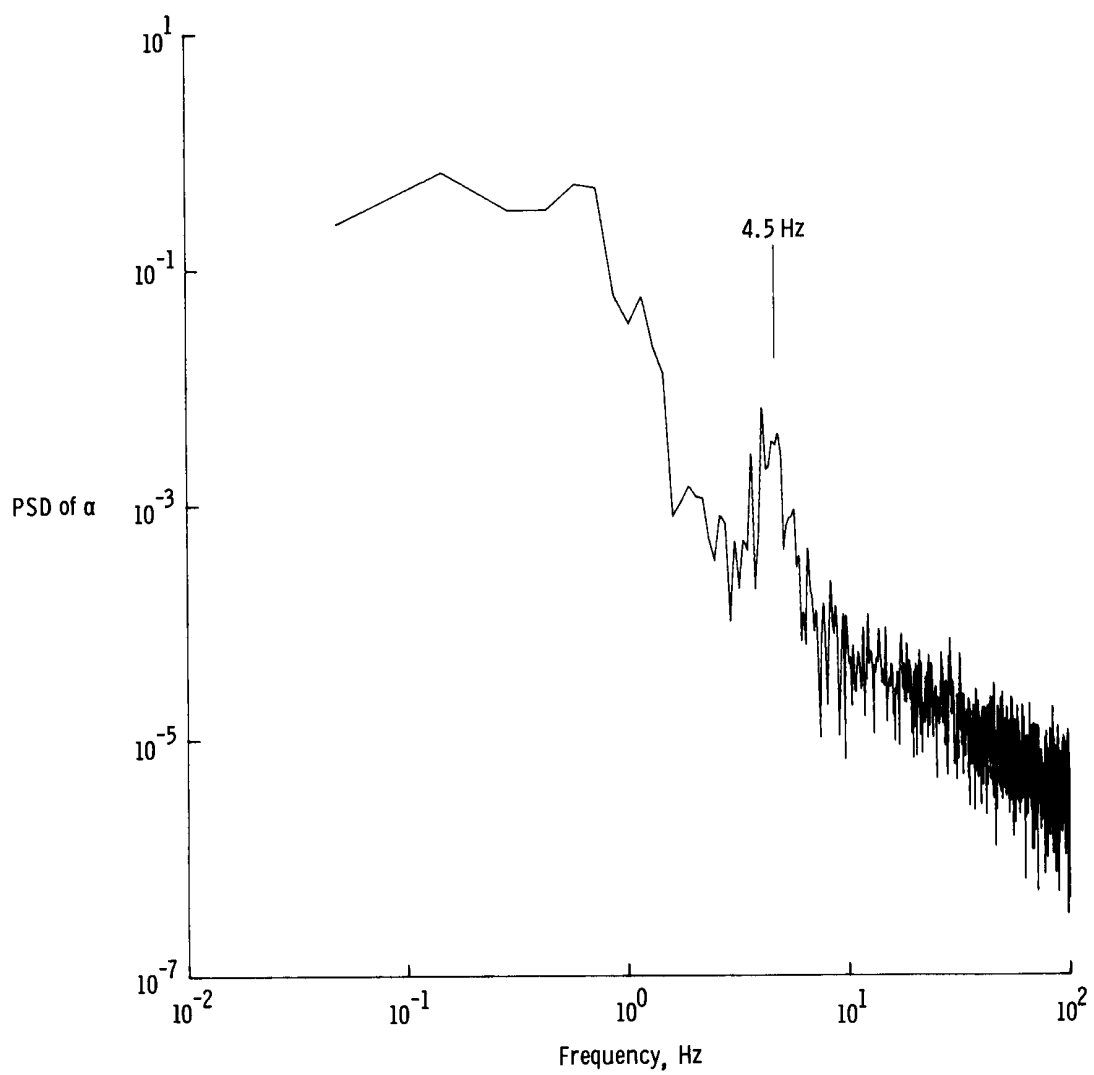
Figure 3. Concluded.
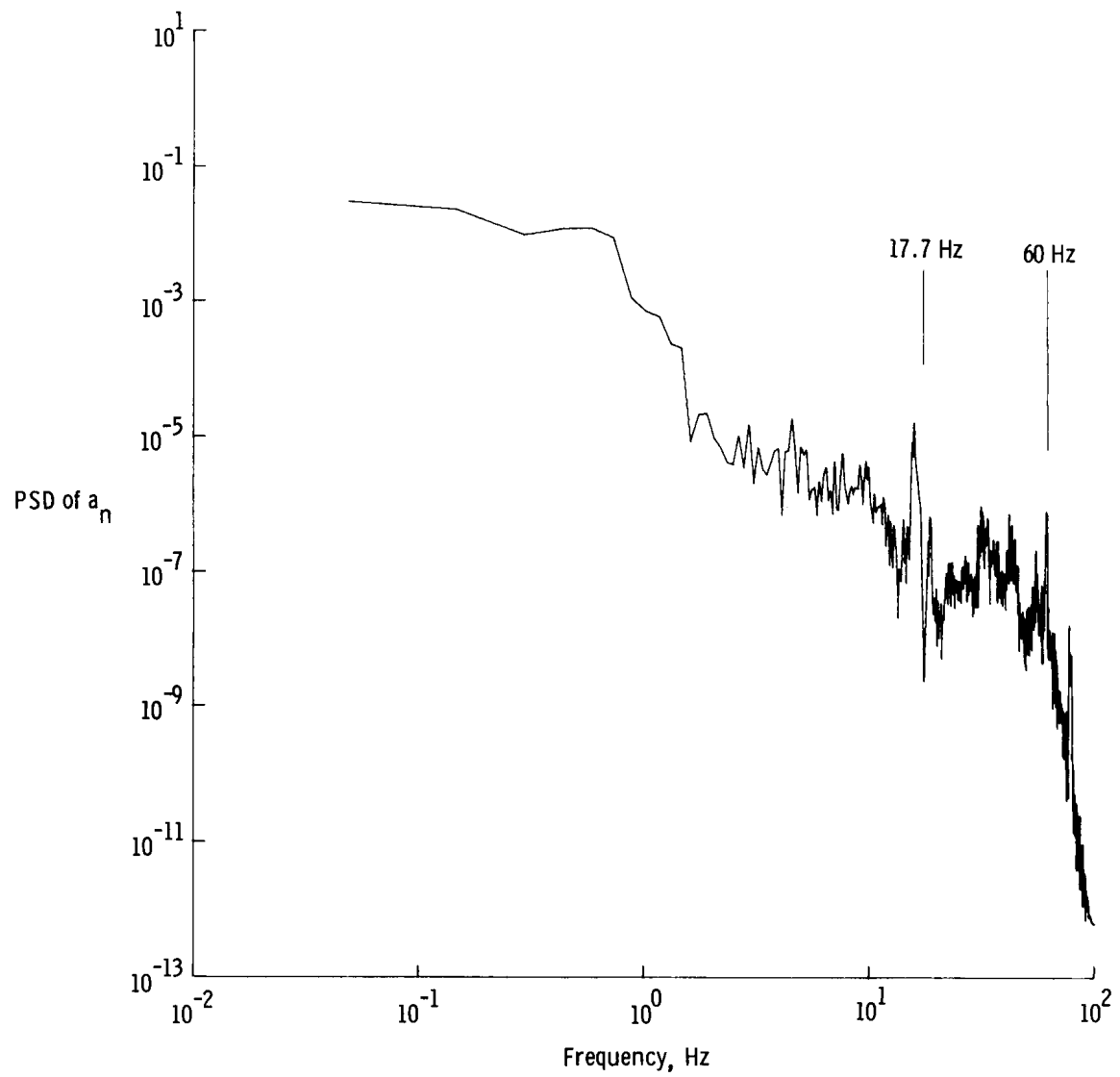
Figure 4. Power spectral densities of filtered 200-sample-per-second data.
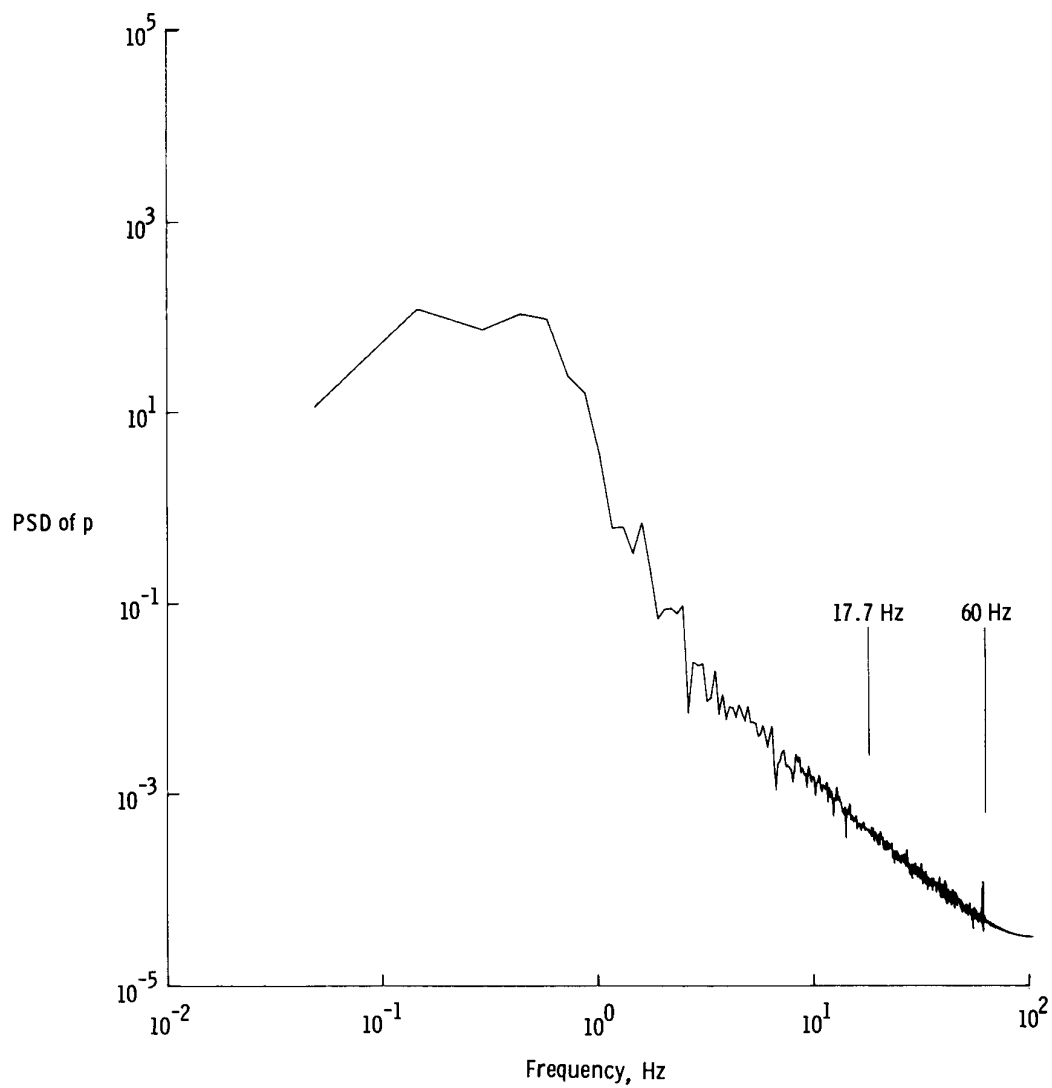
Figure 4. Continued.
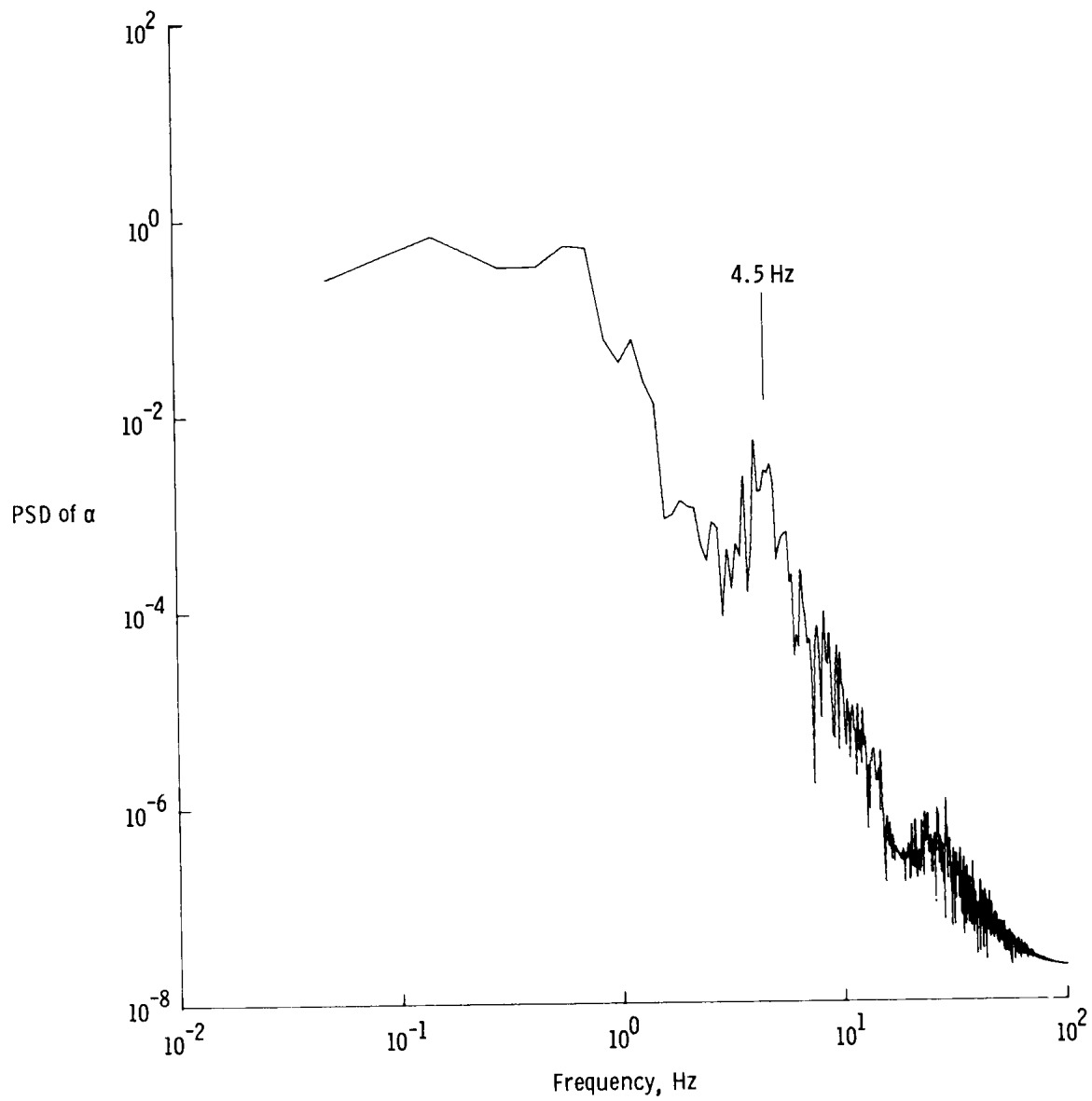
Figure 4. Concluded.
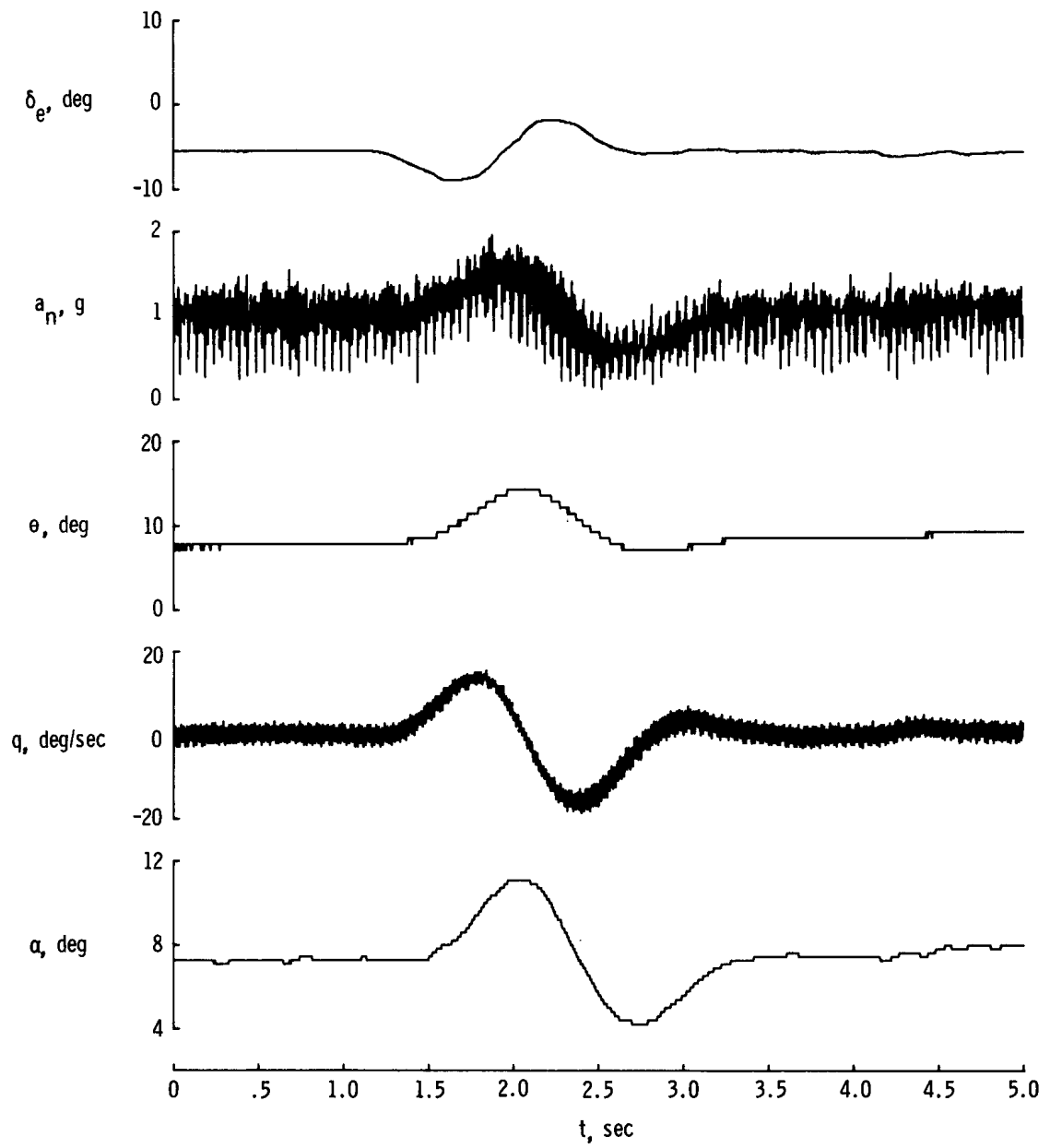
Figure 5. Time history of unfiltered longitudinal data.
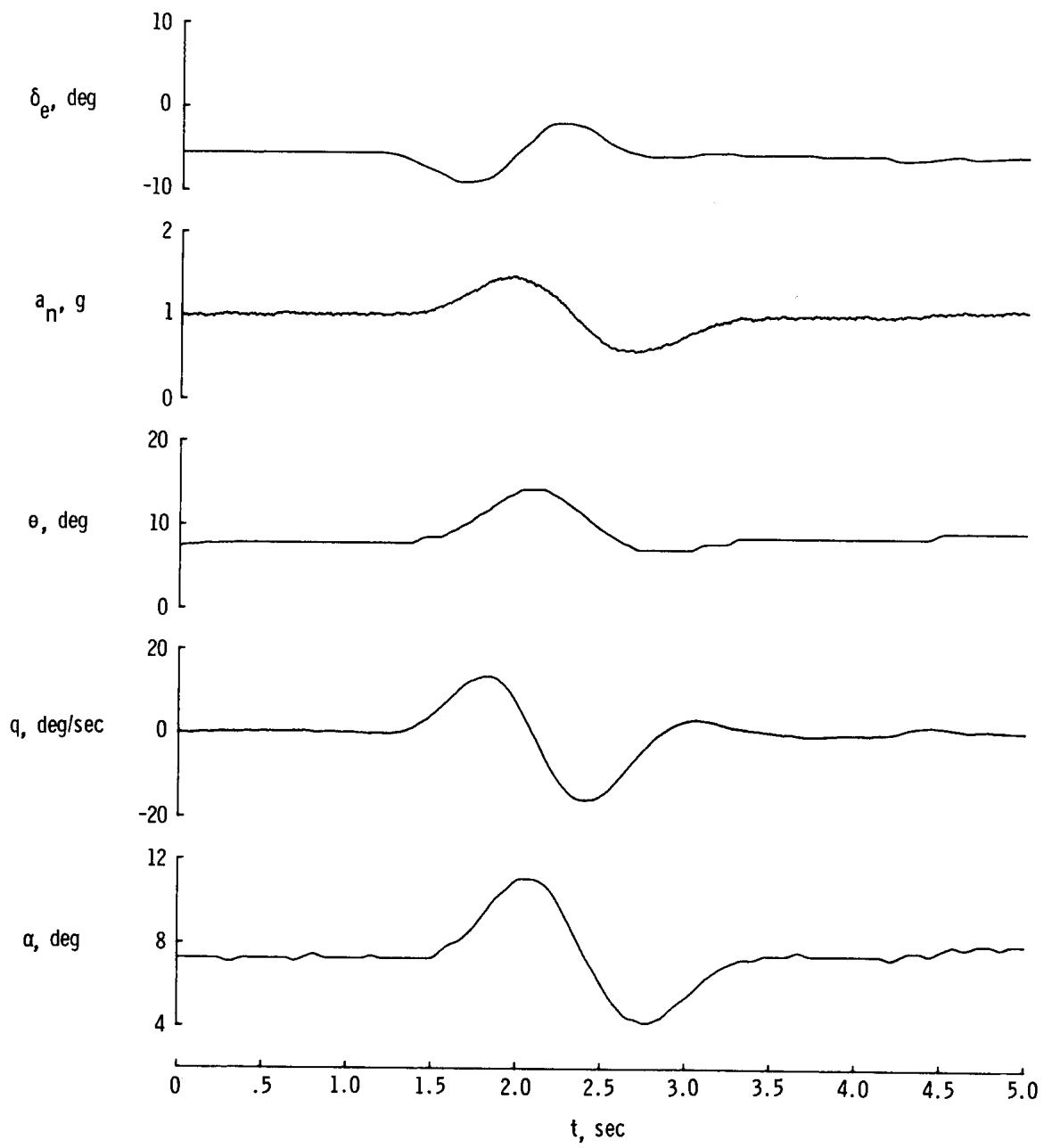
Figure 6. Time history of filtered longitudinal data.
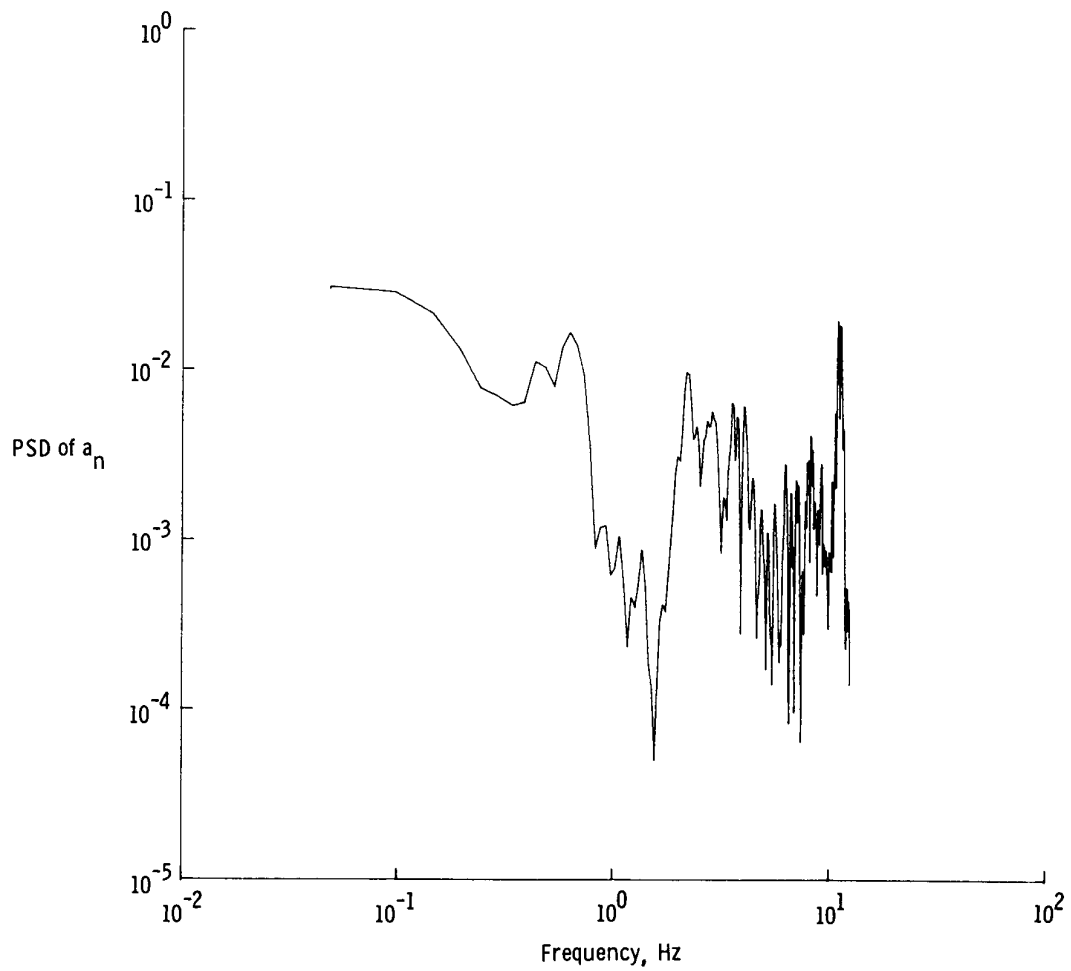
Figure 7. Power spectral density of unfiltered 25-sample-per-second normal acceleration.
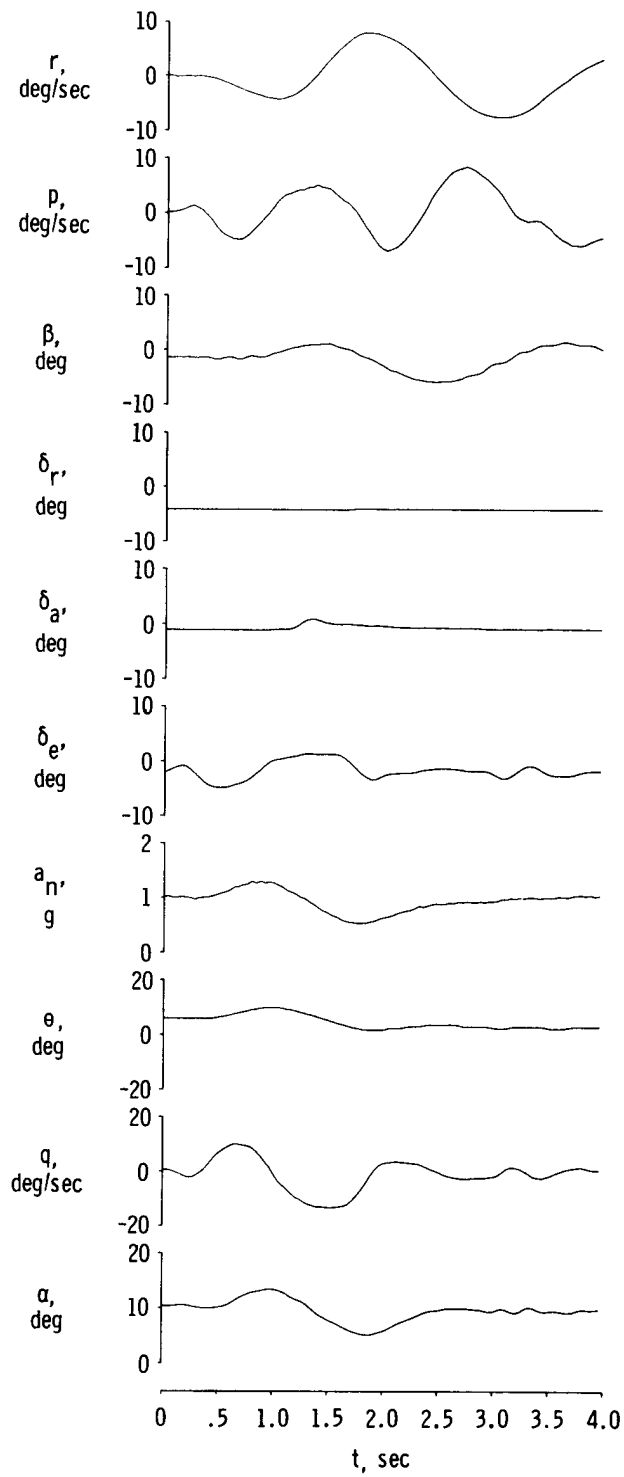
Figure 8. Response of oblique wing aircraft with 45° of wing skew to an elevator pulse.

34
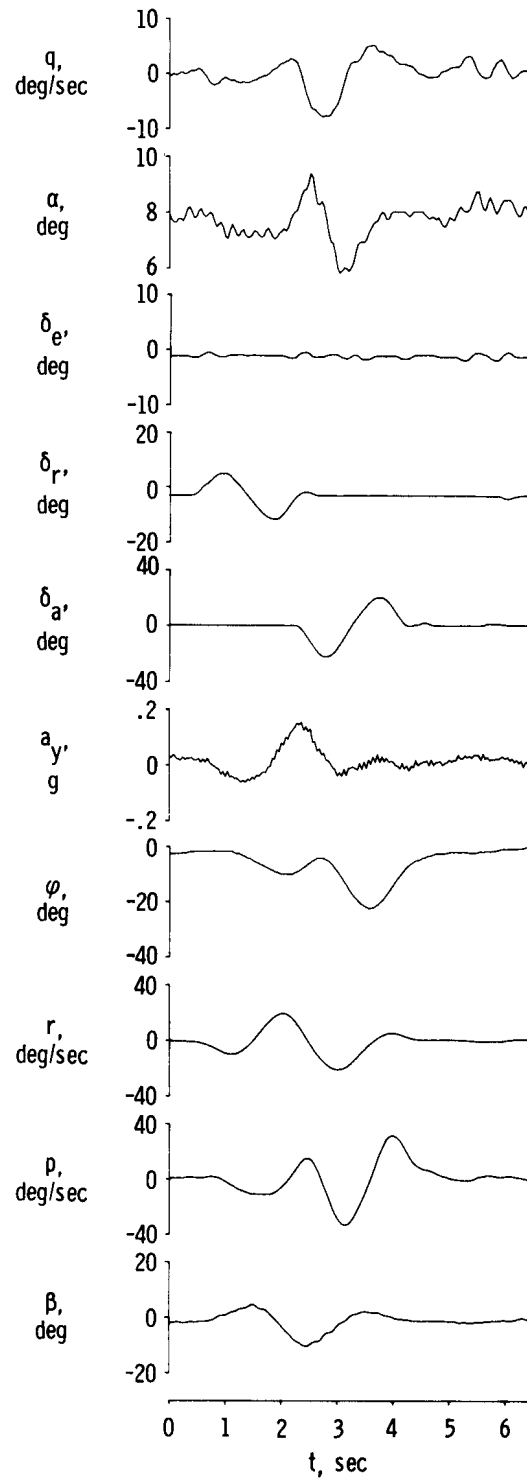
Figure 9. Response of oblique wing aircraft with 45° of wing skew to a maneuver involving rudder and aileron doublets.
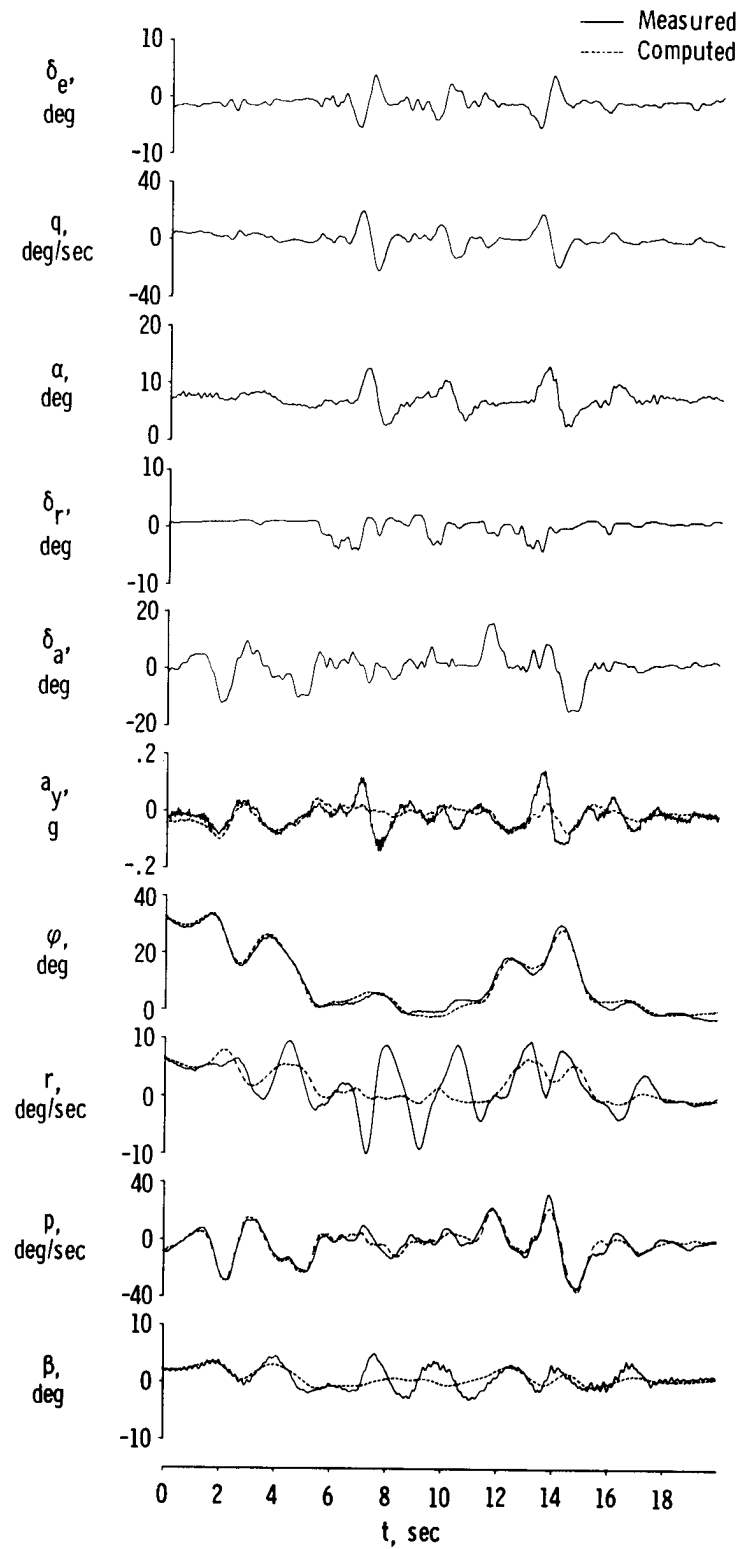
Figure 10. Comparison of measured and computed lateral-directional motions of oblique wing aircraft with 45° of wing skew and cross-coupling terms omitted.
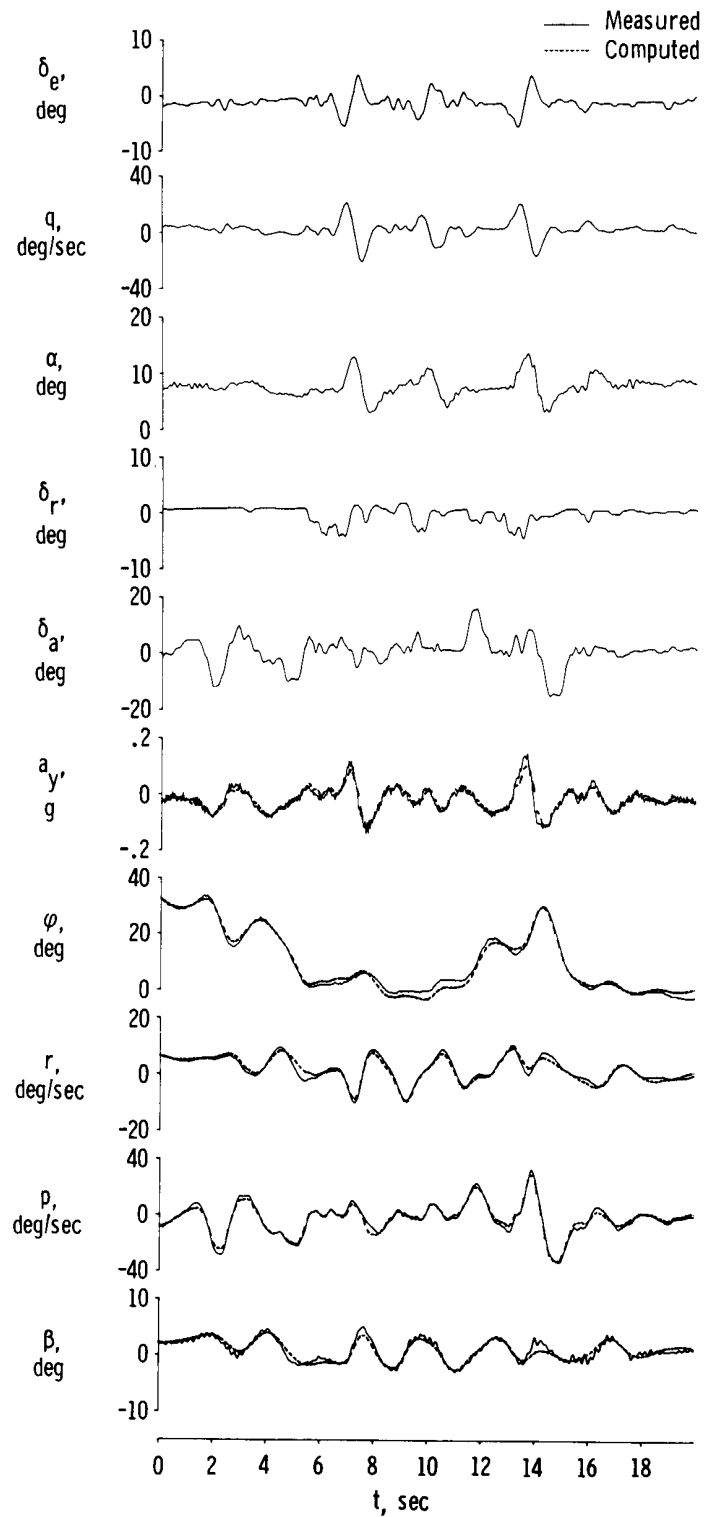
Figure 11. Comparison of measured and computed lateral-directional motions of oblique wing aircraft with 45° of wing skew and cross-coupling terms included.
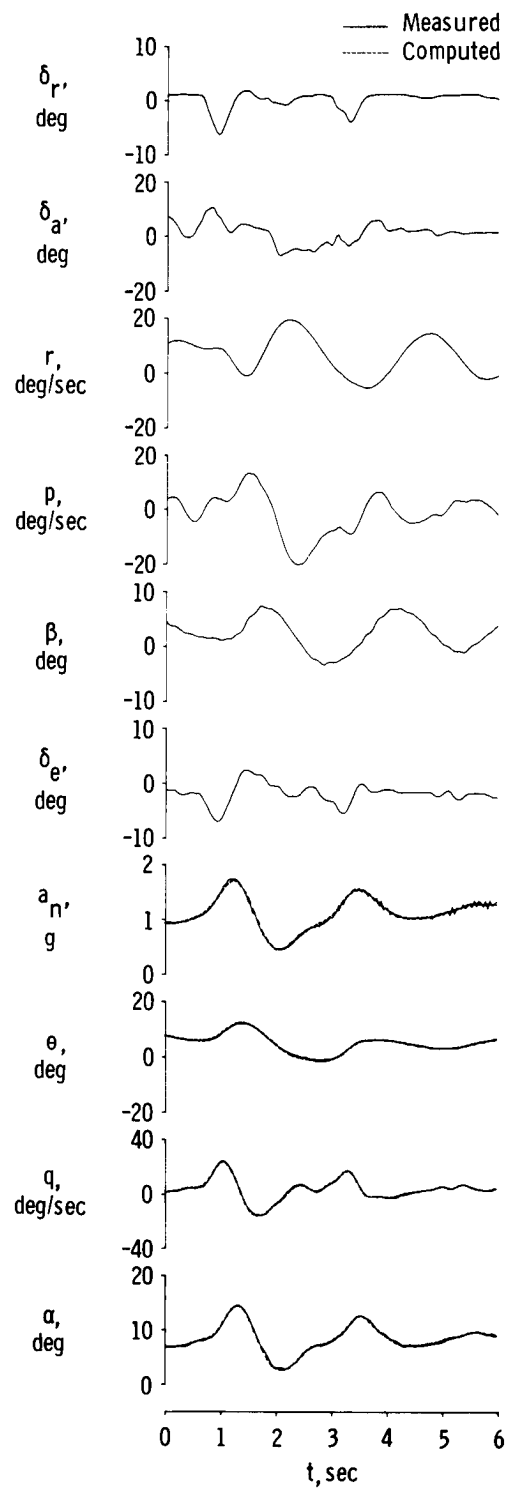
Figure 12. Comparison of measured and computed longitudinal motions of oblique wing aircraft with 45° of wing skew and cross-coupling terms included.
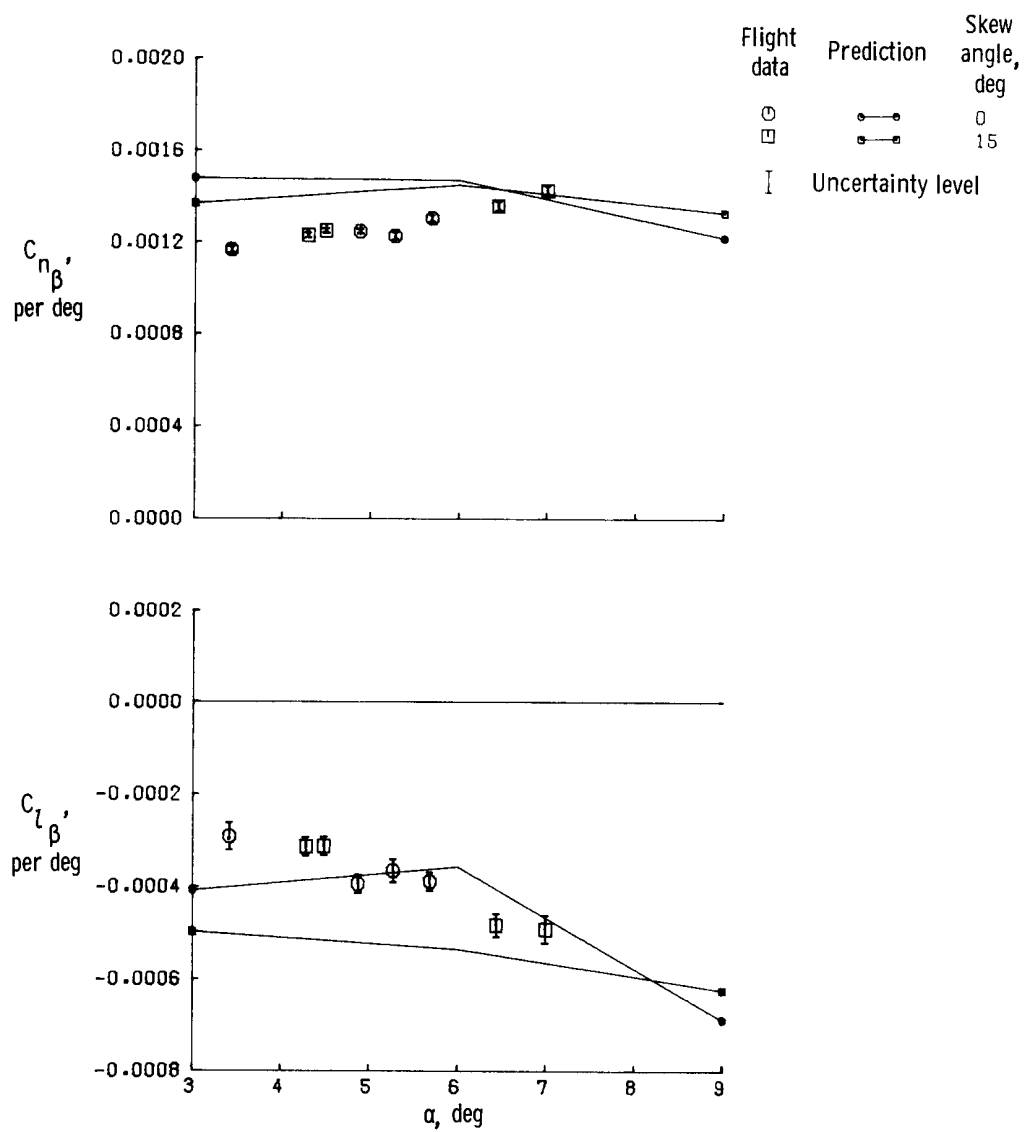
Figure 13. Lateral-directional derivatives of oblique wing aircraft in short tail configuration.
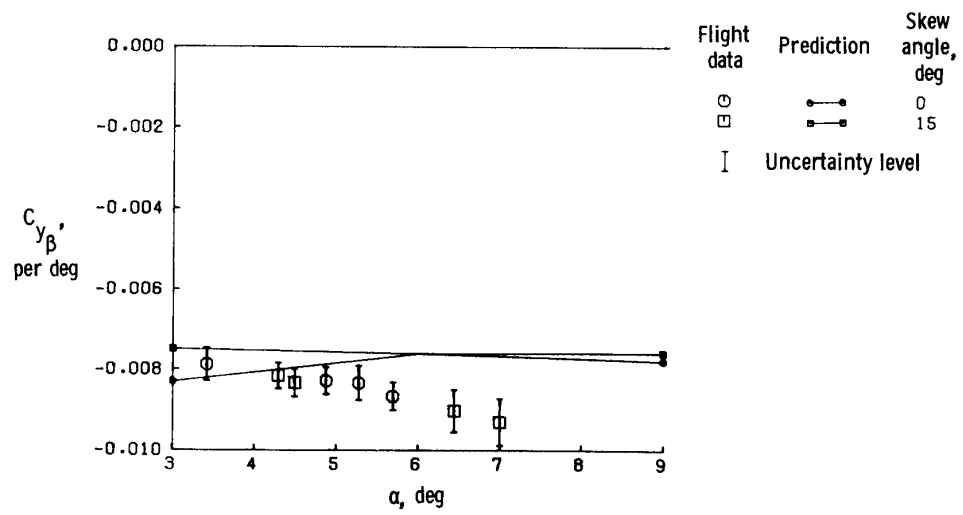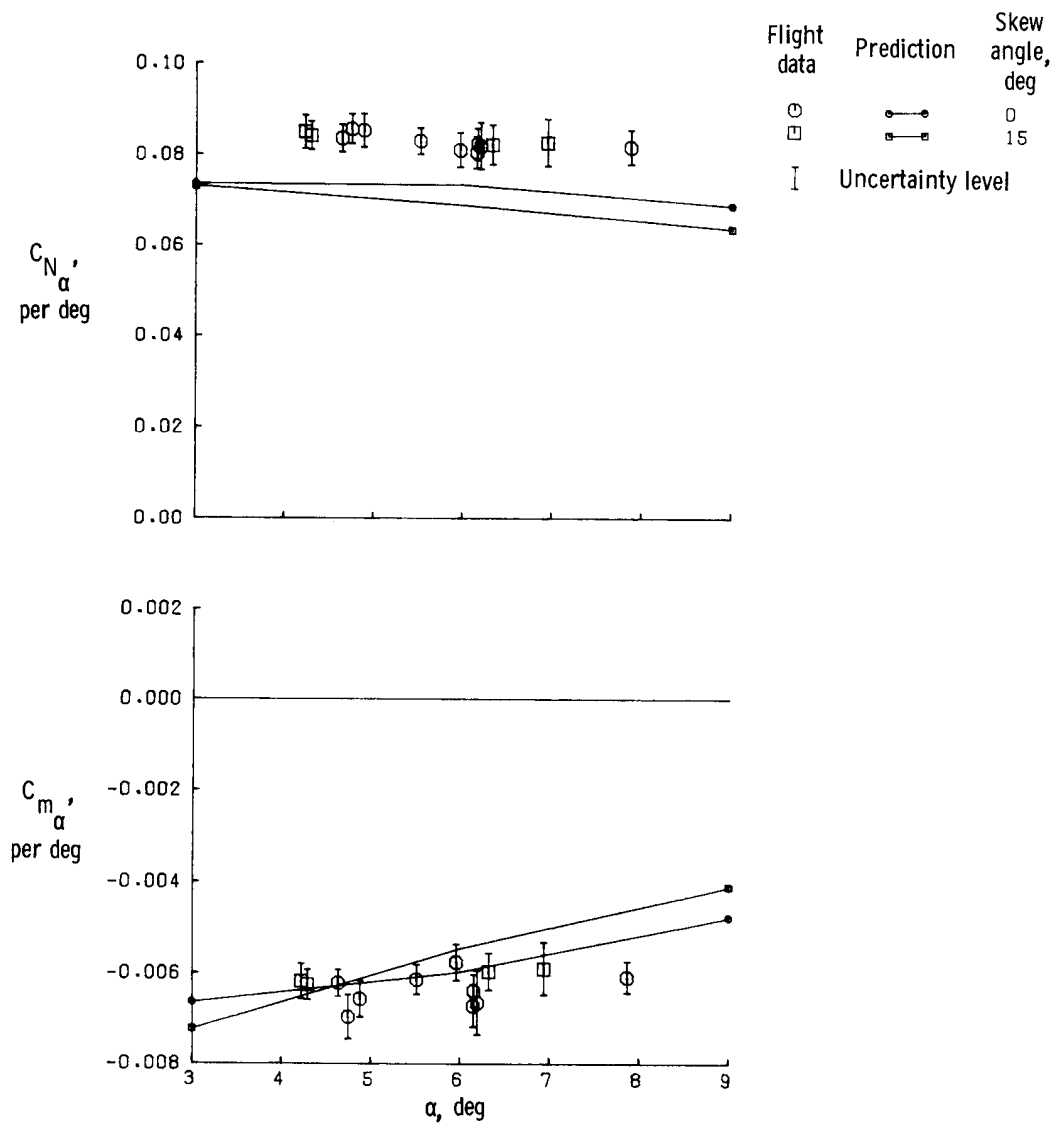
Figure 13. Continued.
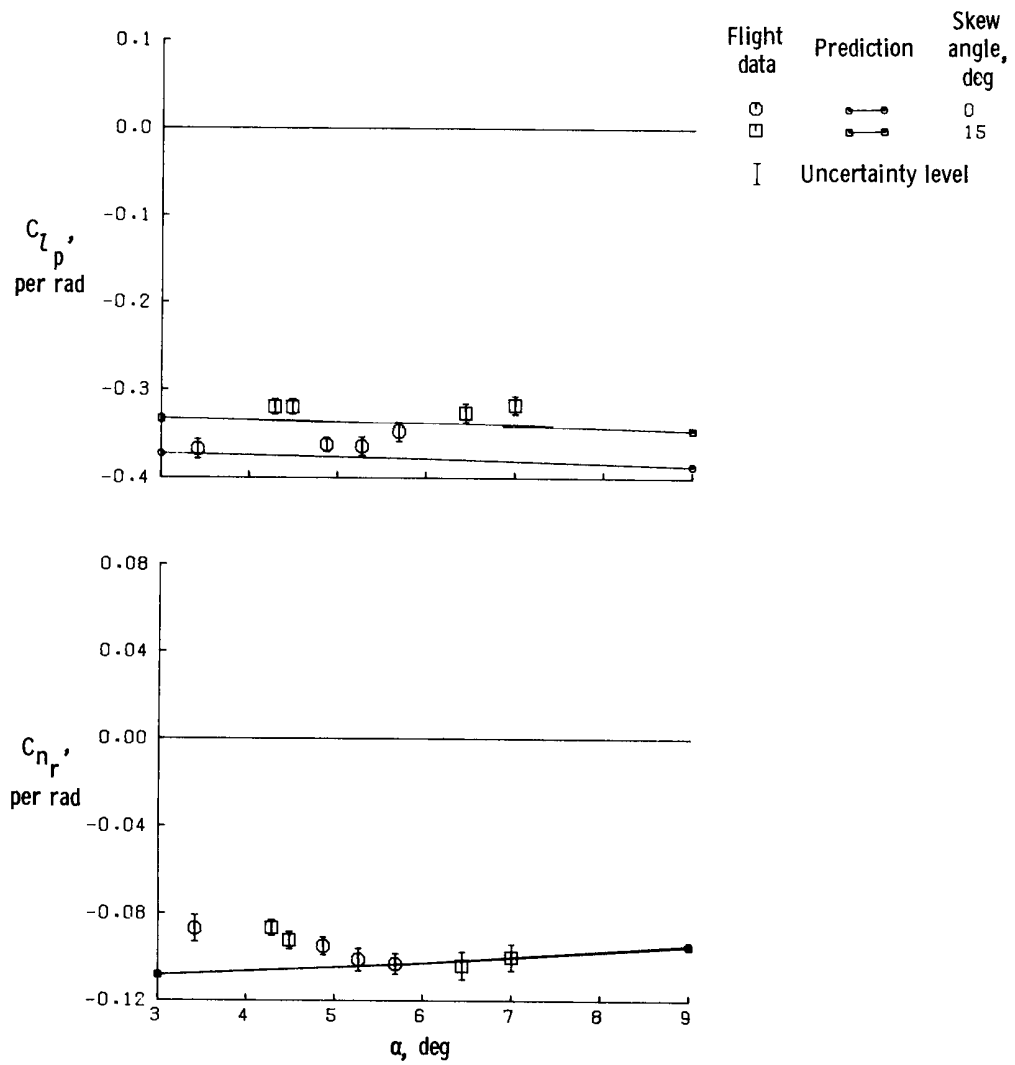
40

Figure 13. Continued.
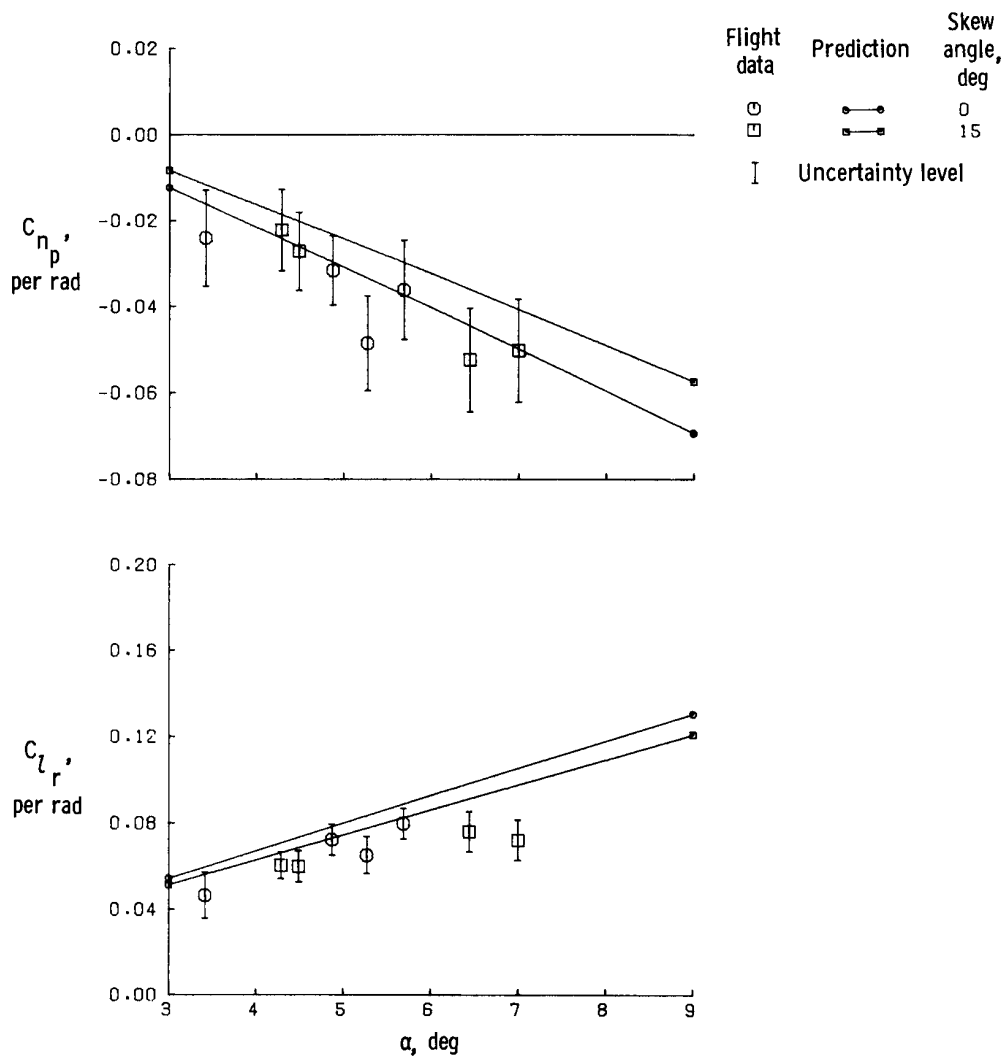
Figure 13. Continued.
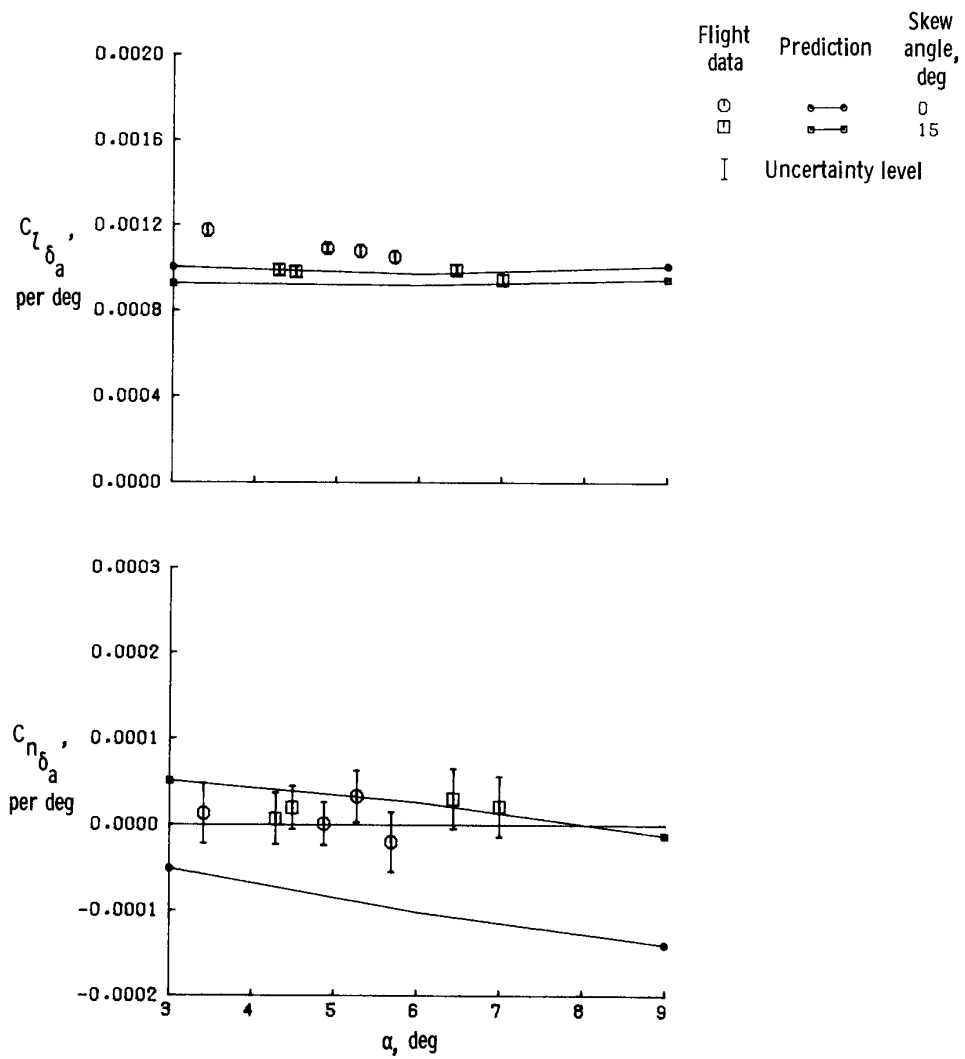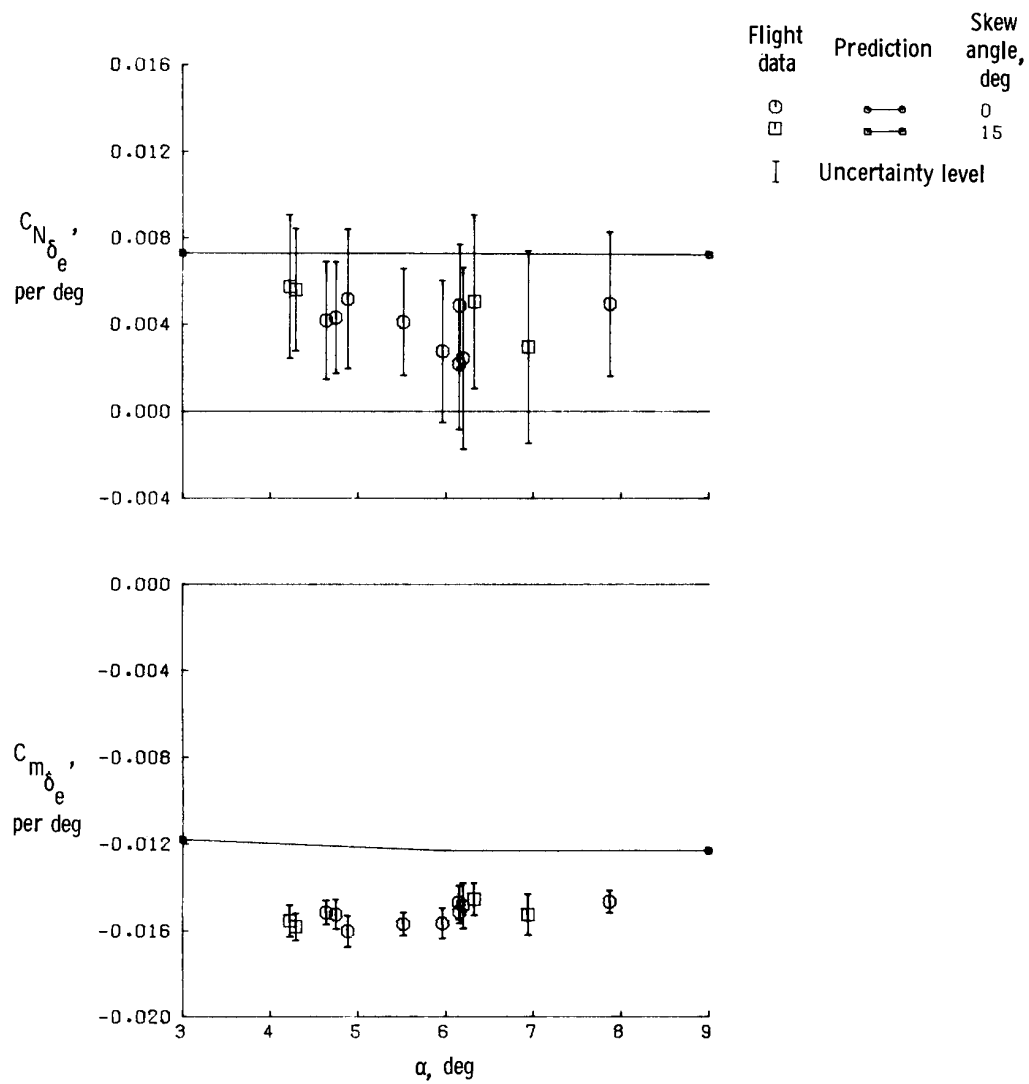
Figure 13. Continued.
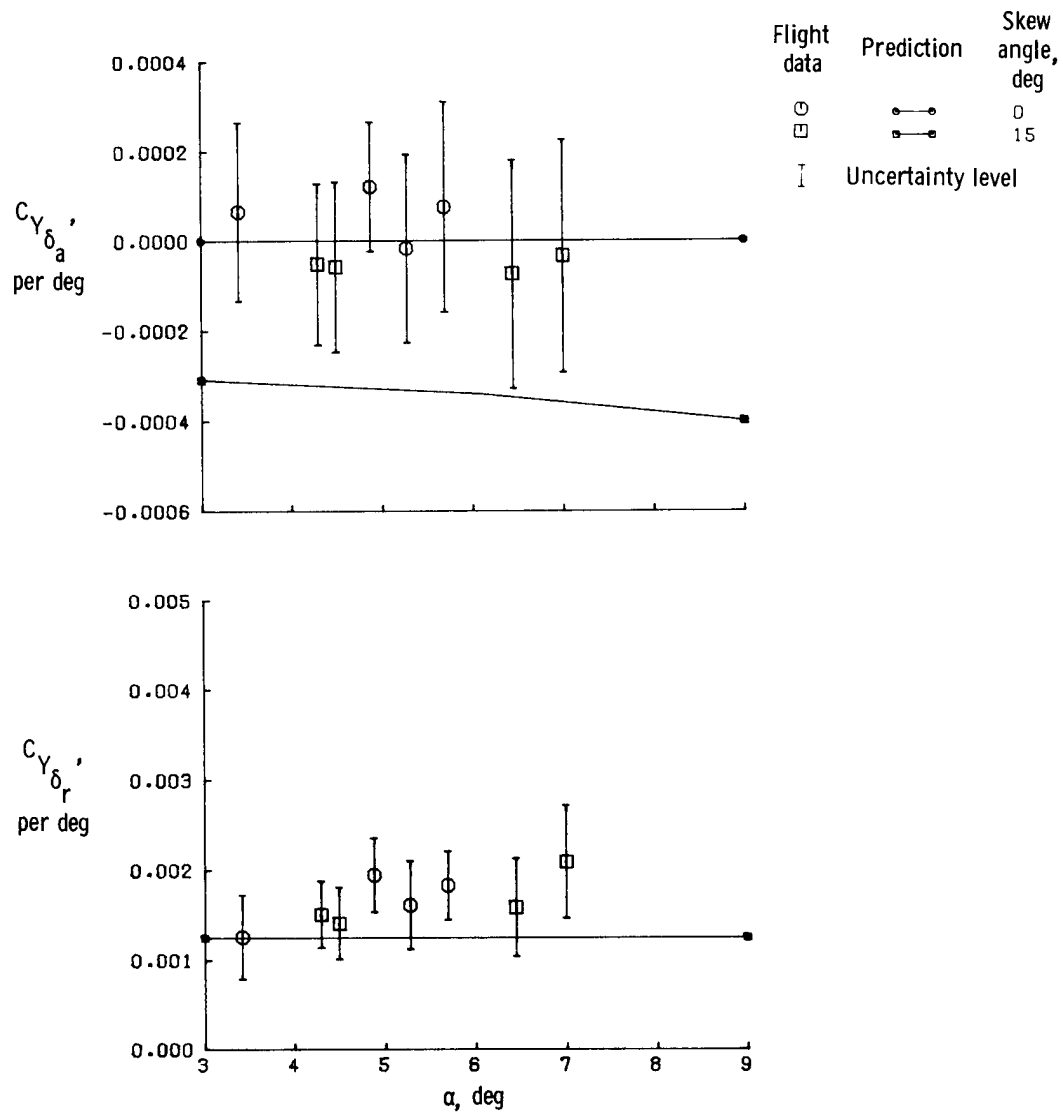
Figure 13. Continued.
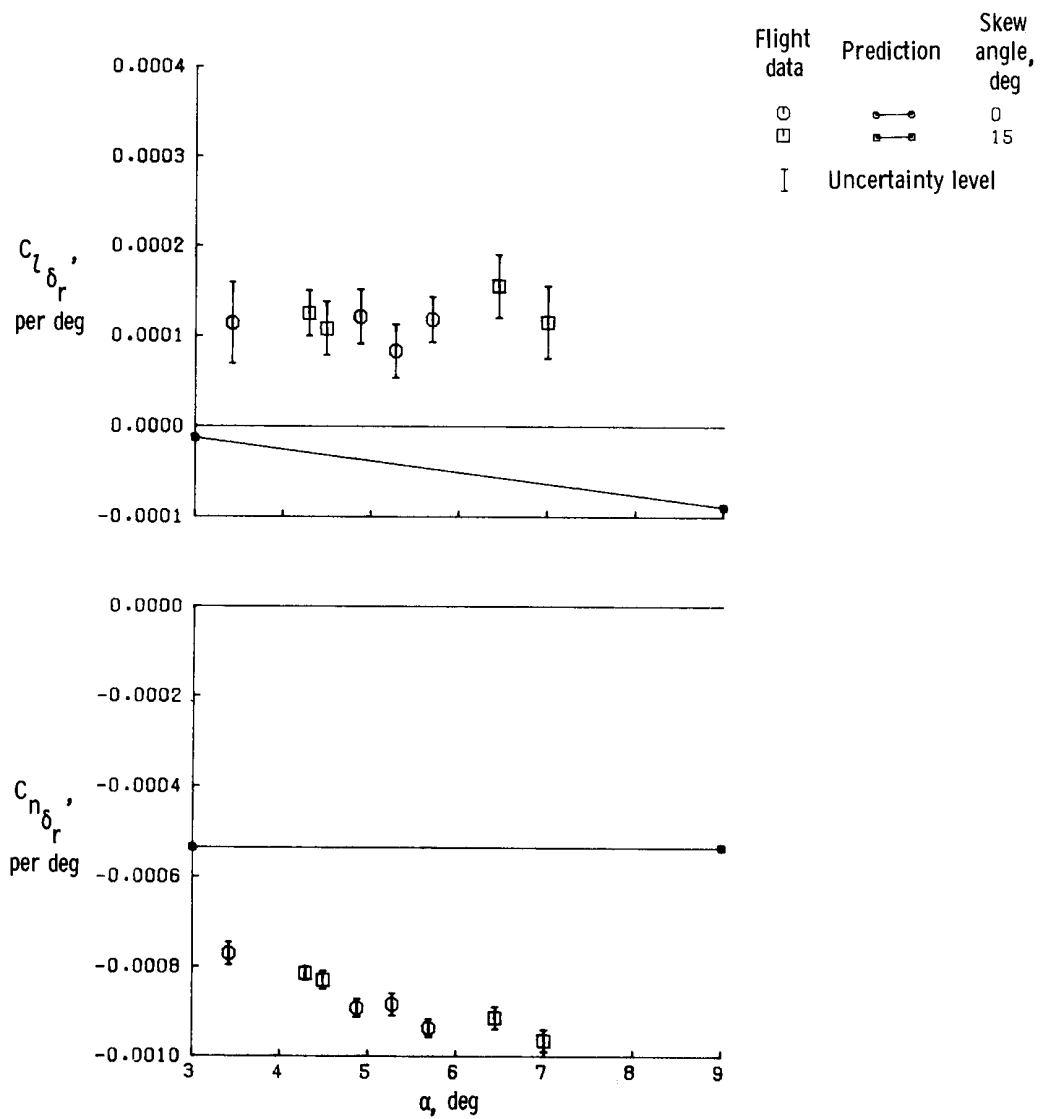
Figure 13. Concluded.
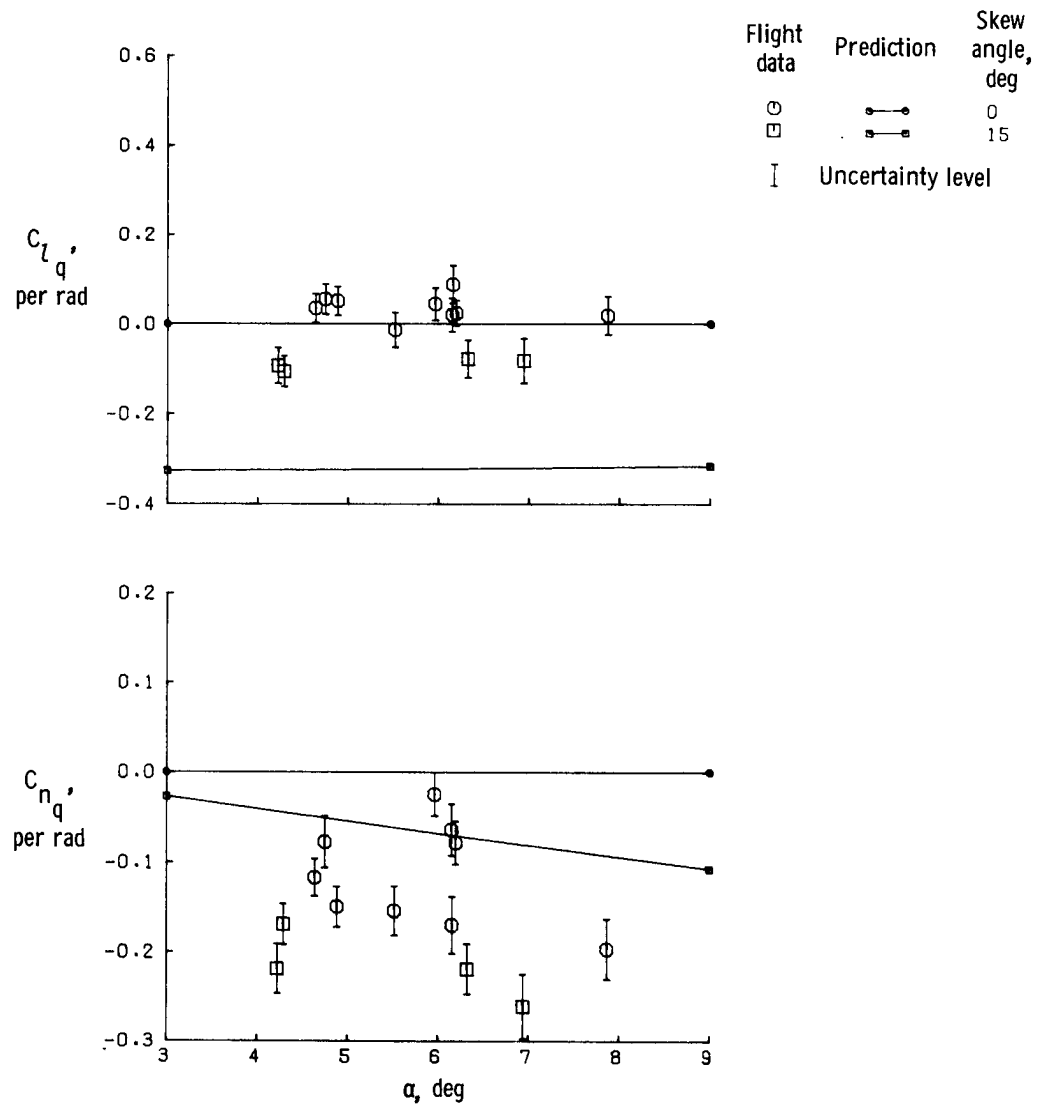
Figure 14. Lateral-directional cross-coupling derivatives of oblique wing aircraft in short tail configuration.
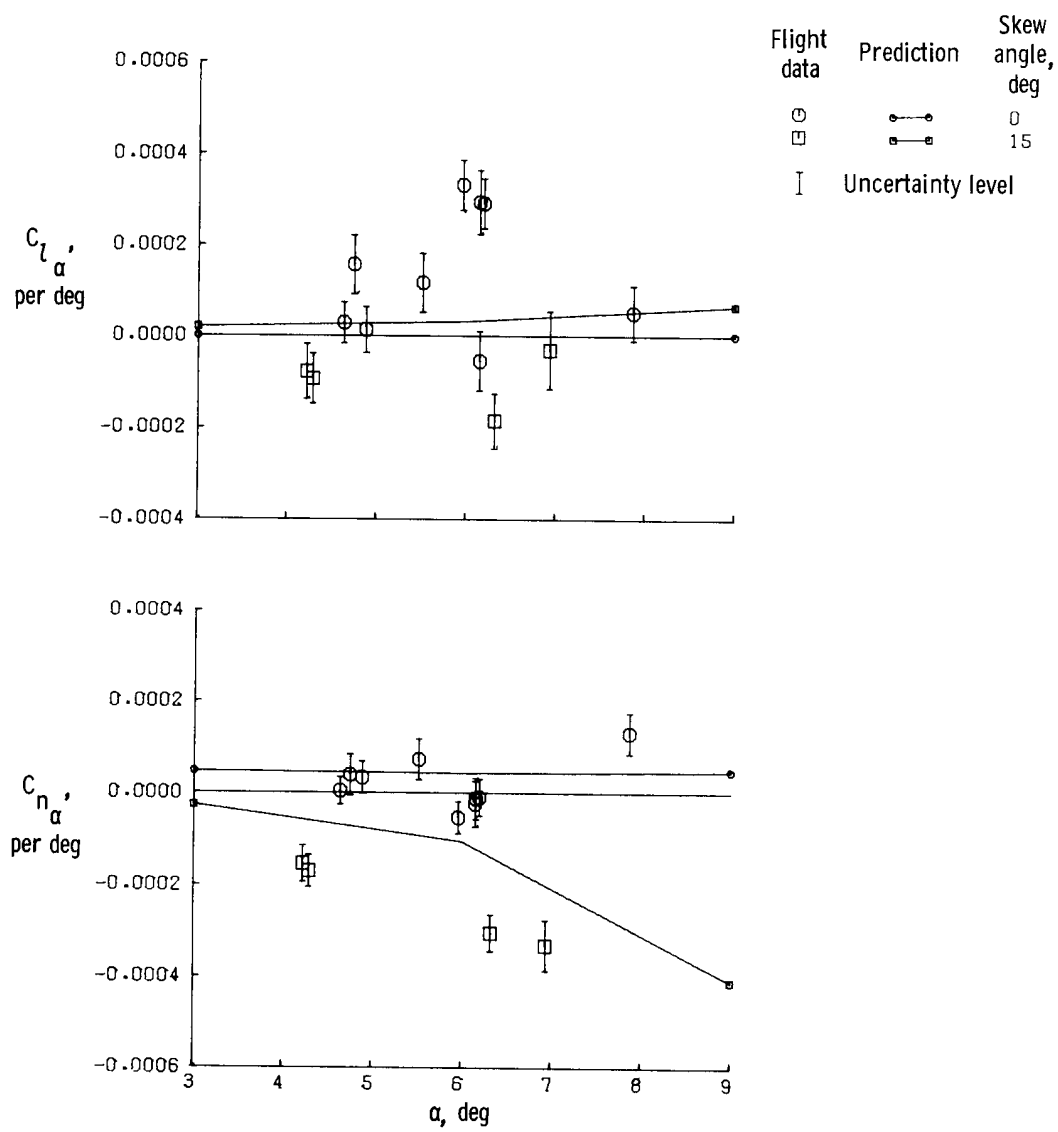
Figure 14. Continued.
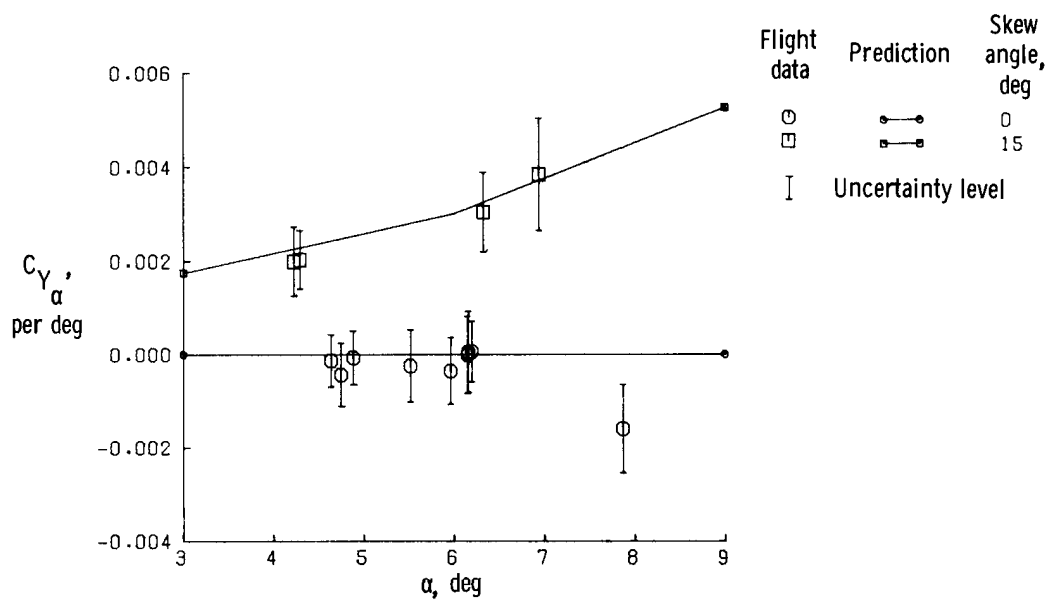
Figure 14. Concluded.

Figure 15. Longitudinal derivatives of oblique wing aircraft in short tail configuration.
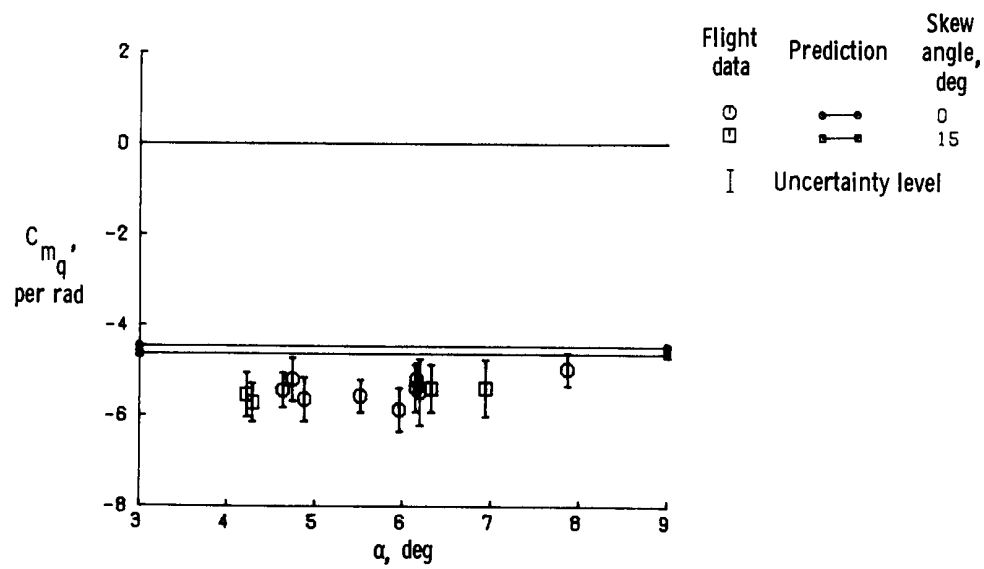
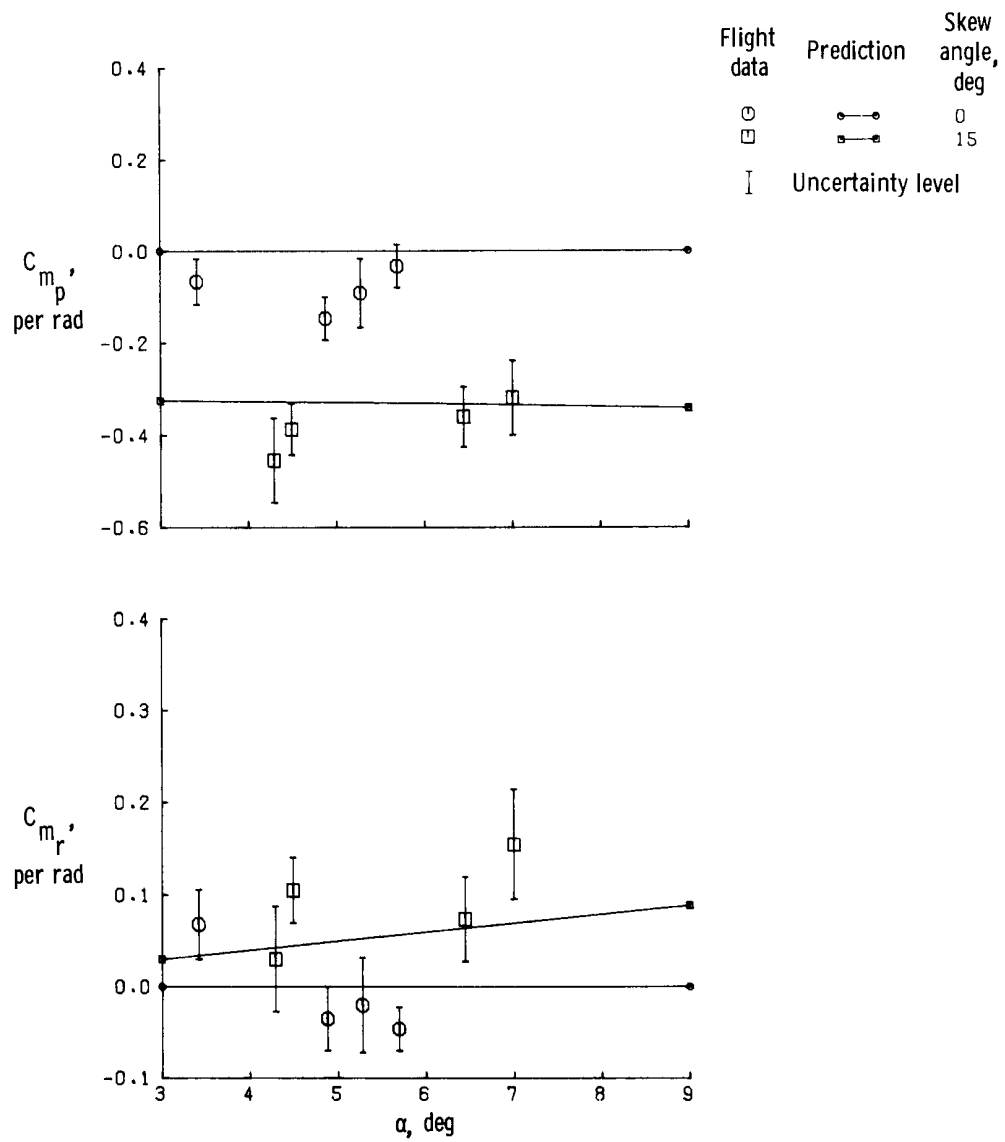*Figure 15. Continued.*

Figure 15. Concluded.

Figure 16. Longitudinal cross-coupling derivatives of oblique wing aircraft in short tail configuration.
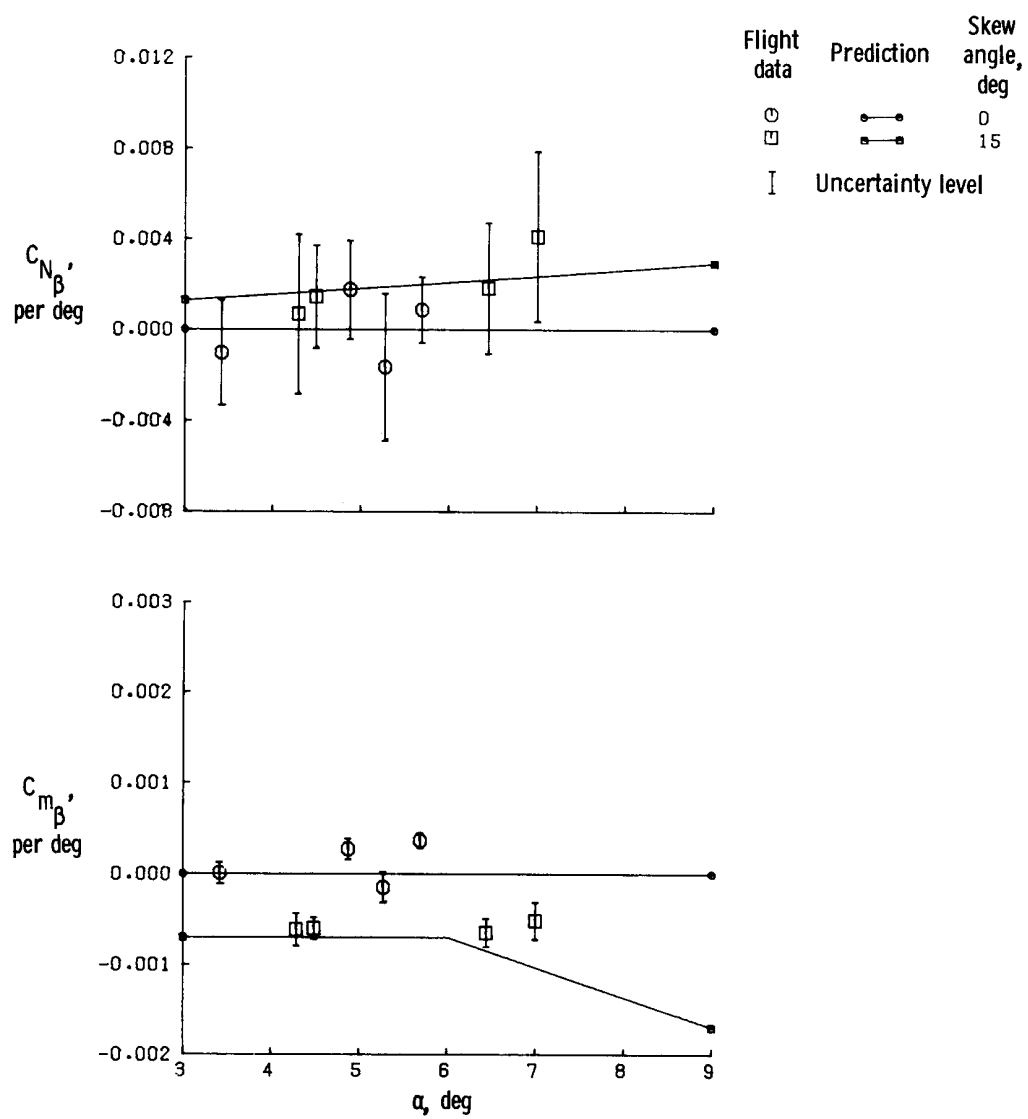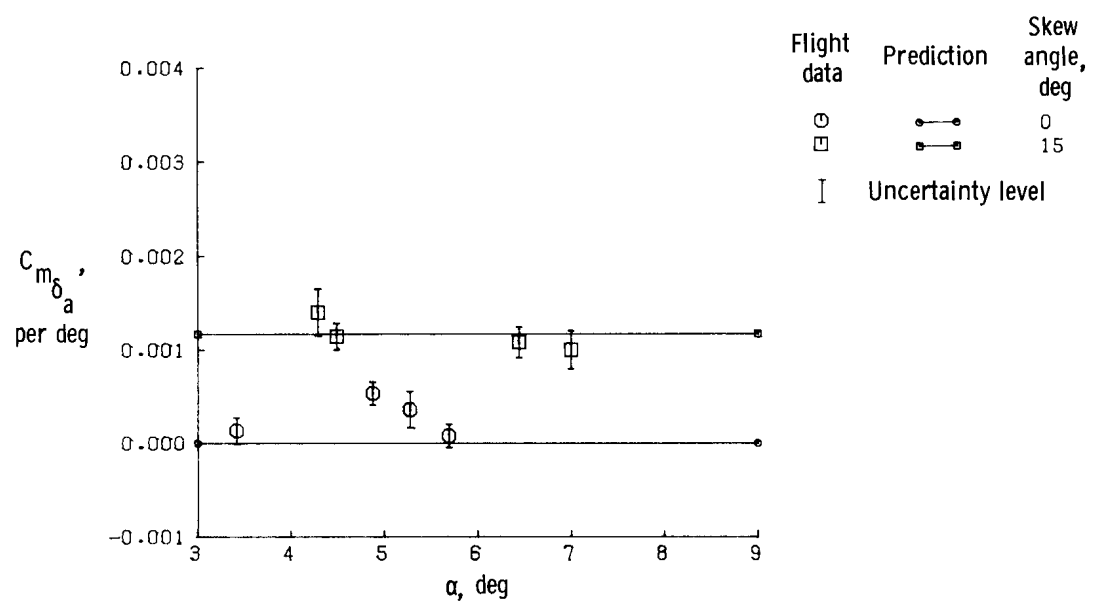
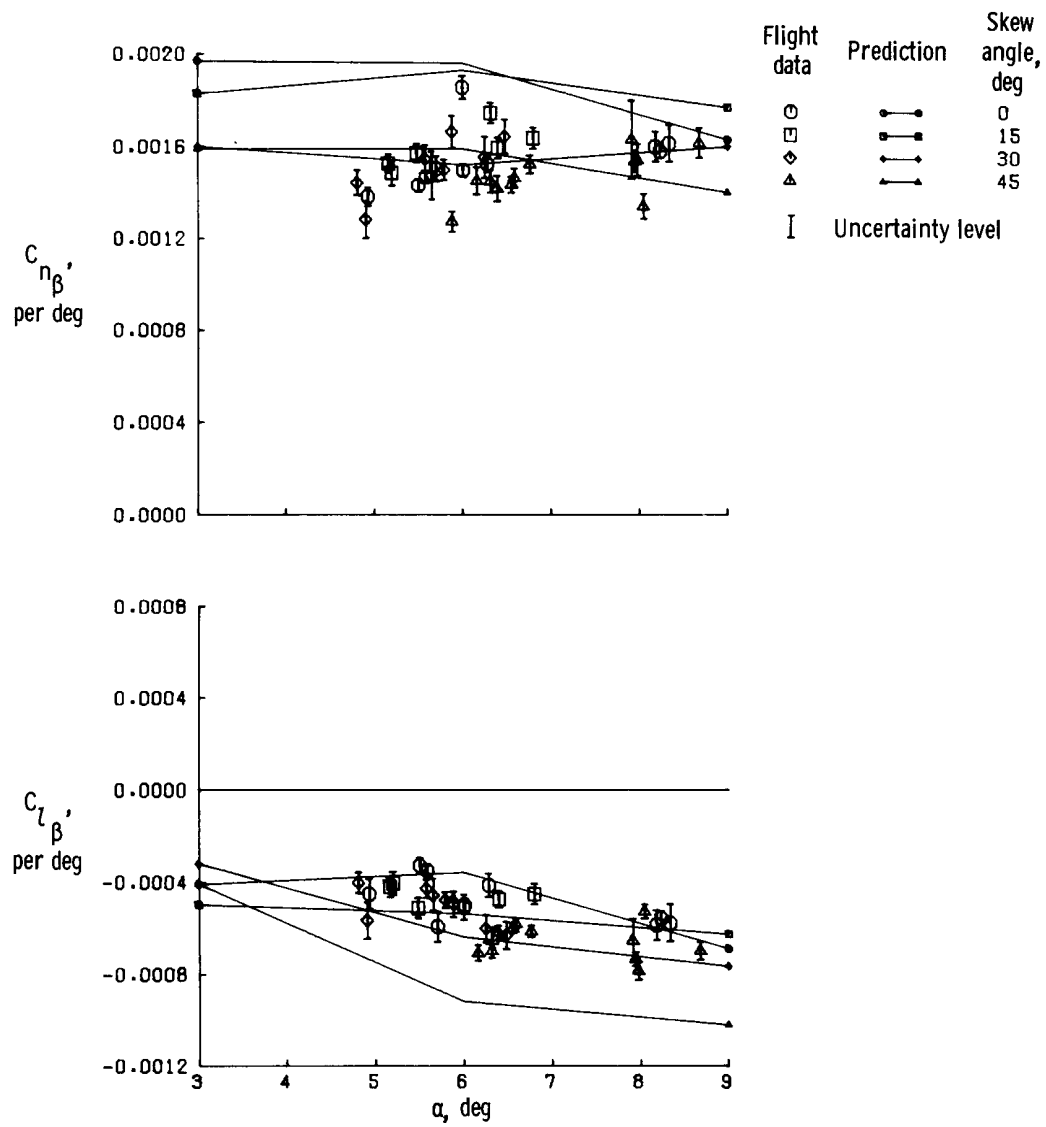*Figure 16. Continued.*

Figure 16. Concluded.

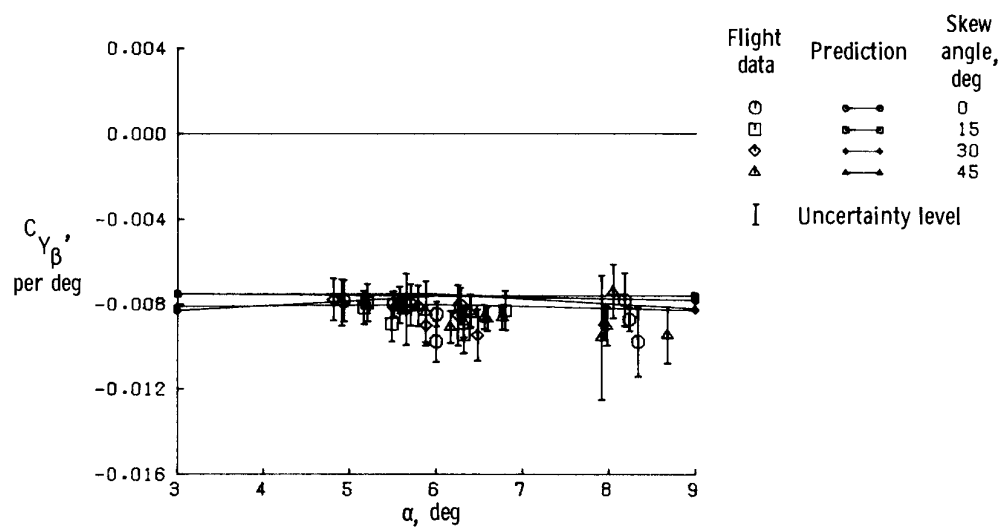*Figure 17. Lateral-directional derivatives of oblique wing aircraft in long tail configuration.*

Figure 17. Continued.

Figure 17. Continued.

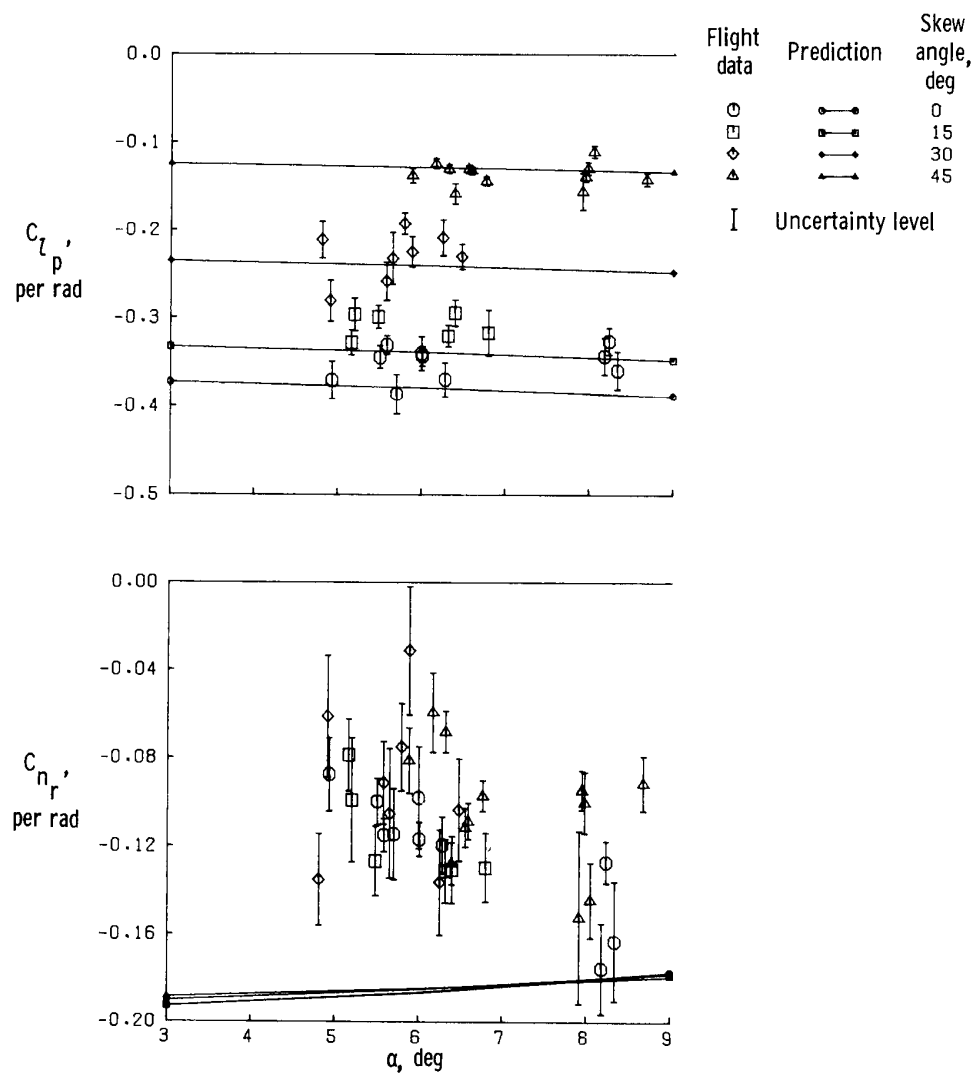Figure 17. Continued.

Figure 17. Continued.

Figure 17. Continued.

Figure 17. Concluded.

Figure 18. Lateral-directional cross-coupling derivatives of oblique wing aircraft in long tail configuration.

Figure 18. Continued.

Figure 18. Concluded.

Figure 19. Longitudinal derivatives of oblique wing aircraft in long tail configuration.
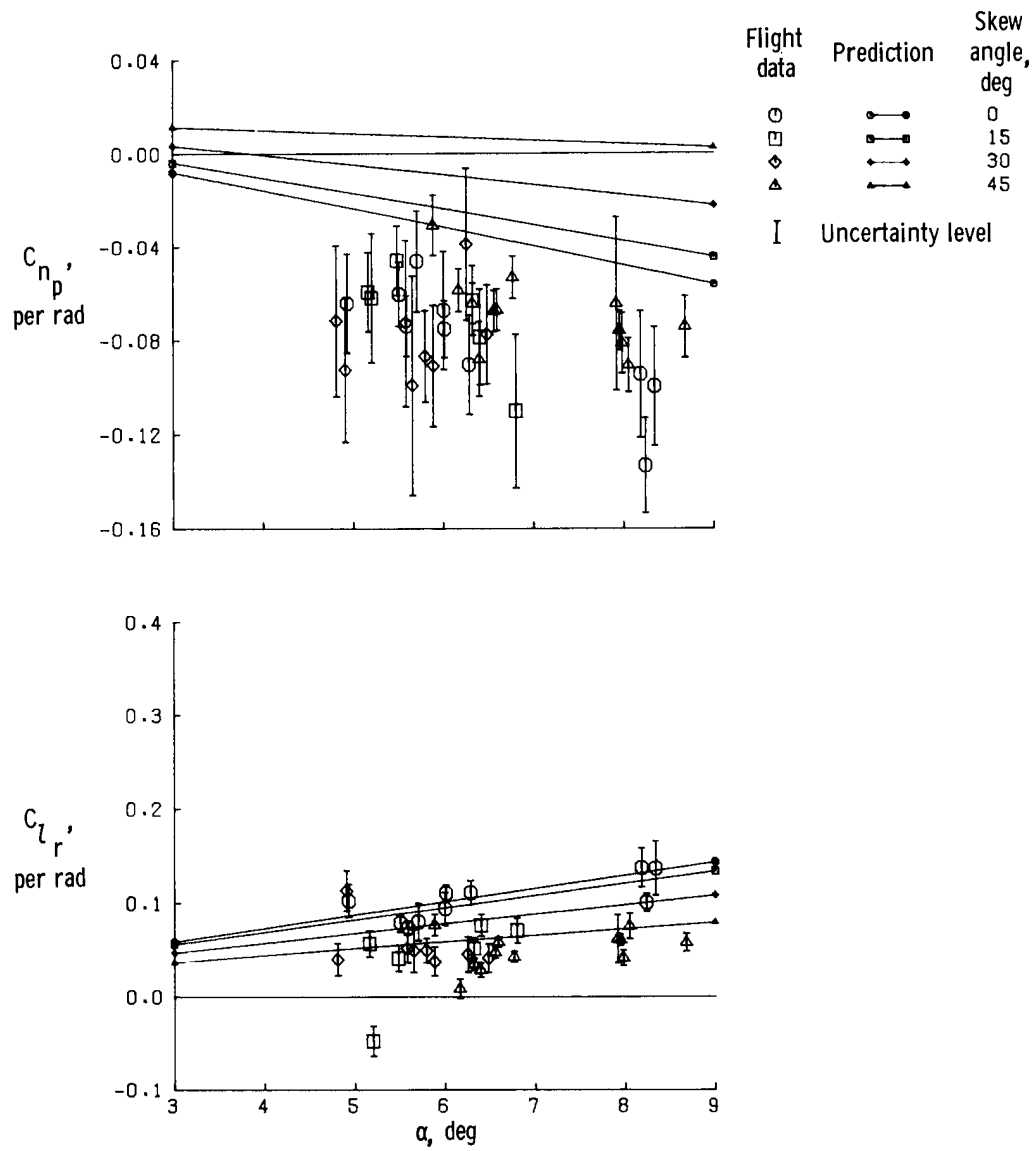
Figure 19. Continued.
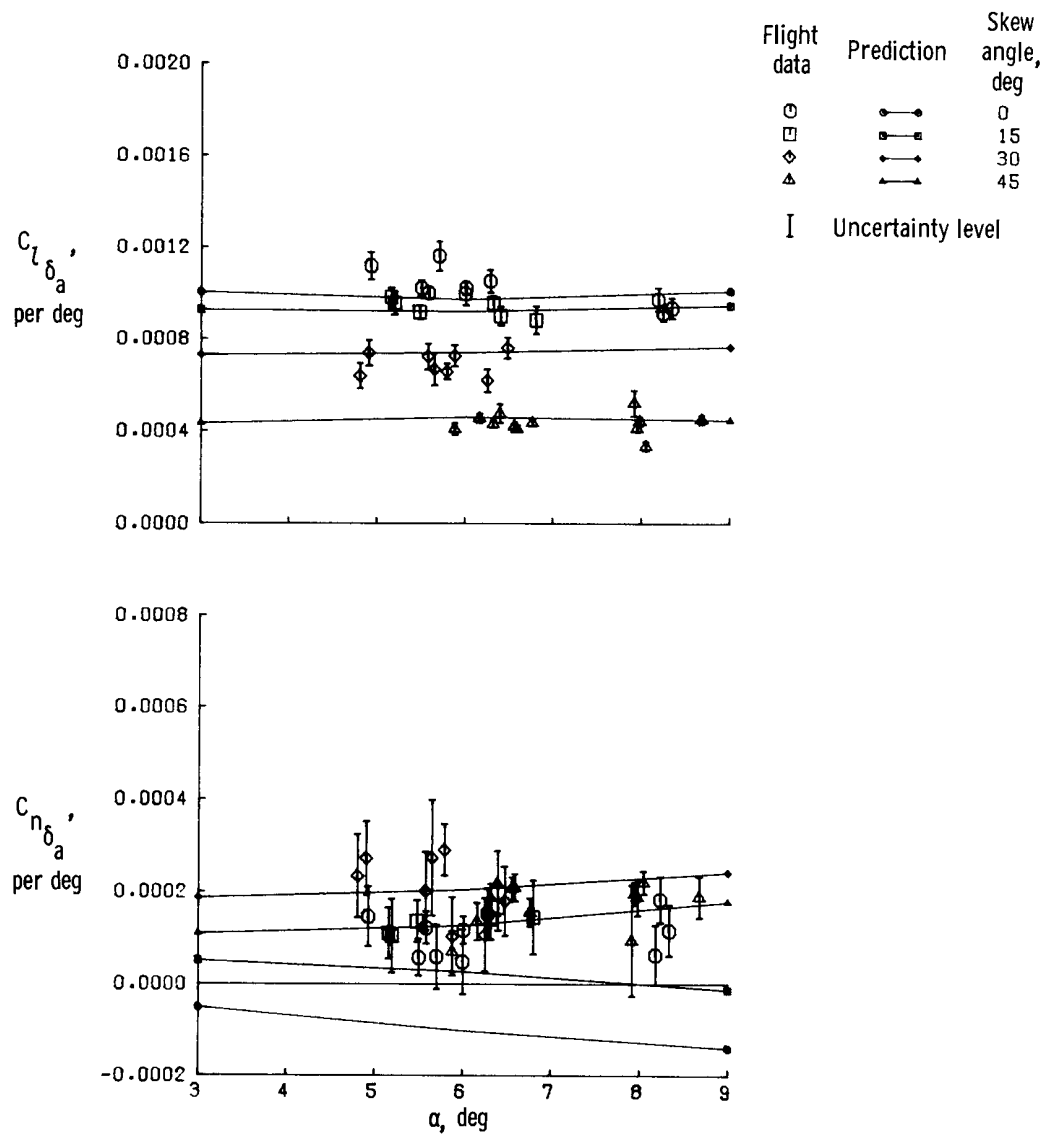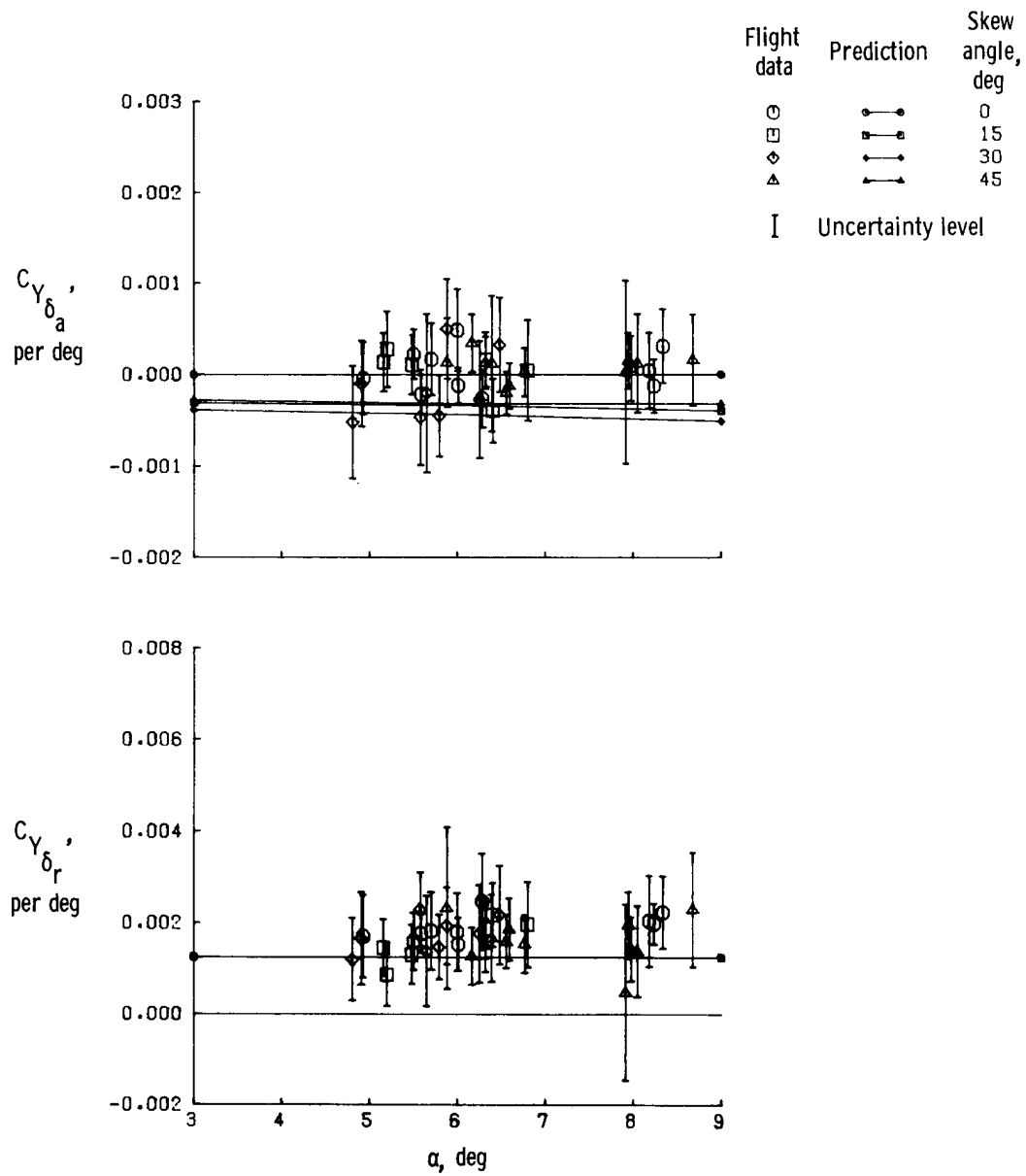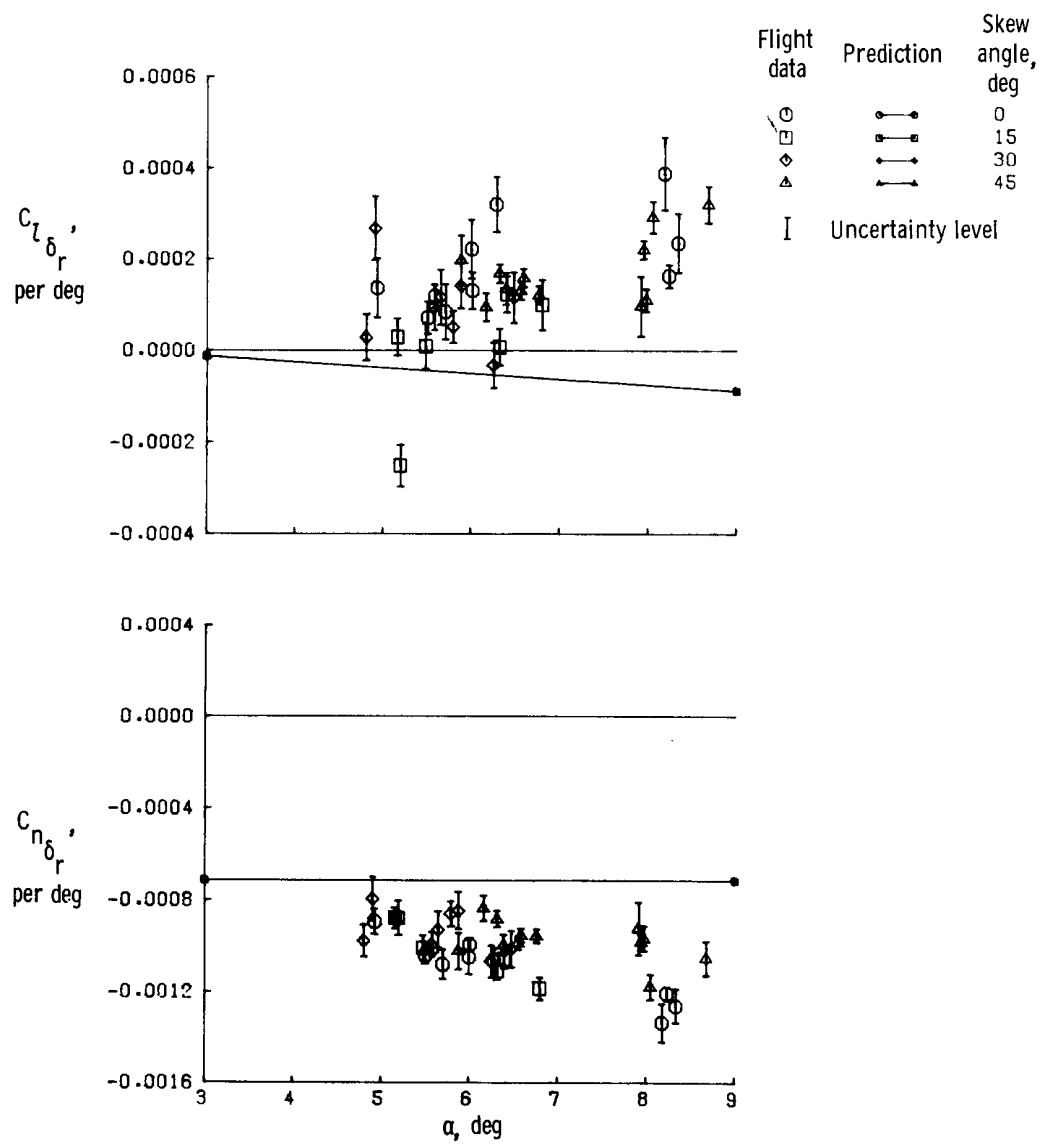
Figure 19. Concluded.

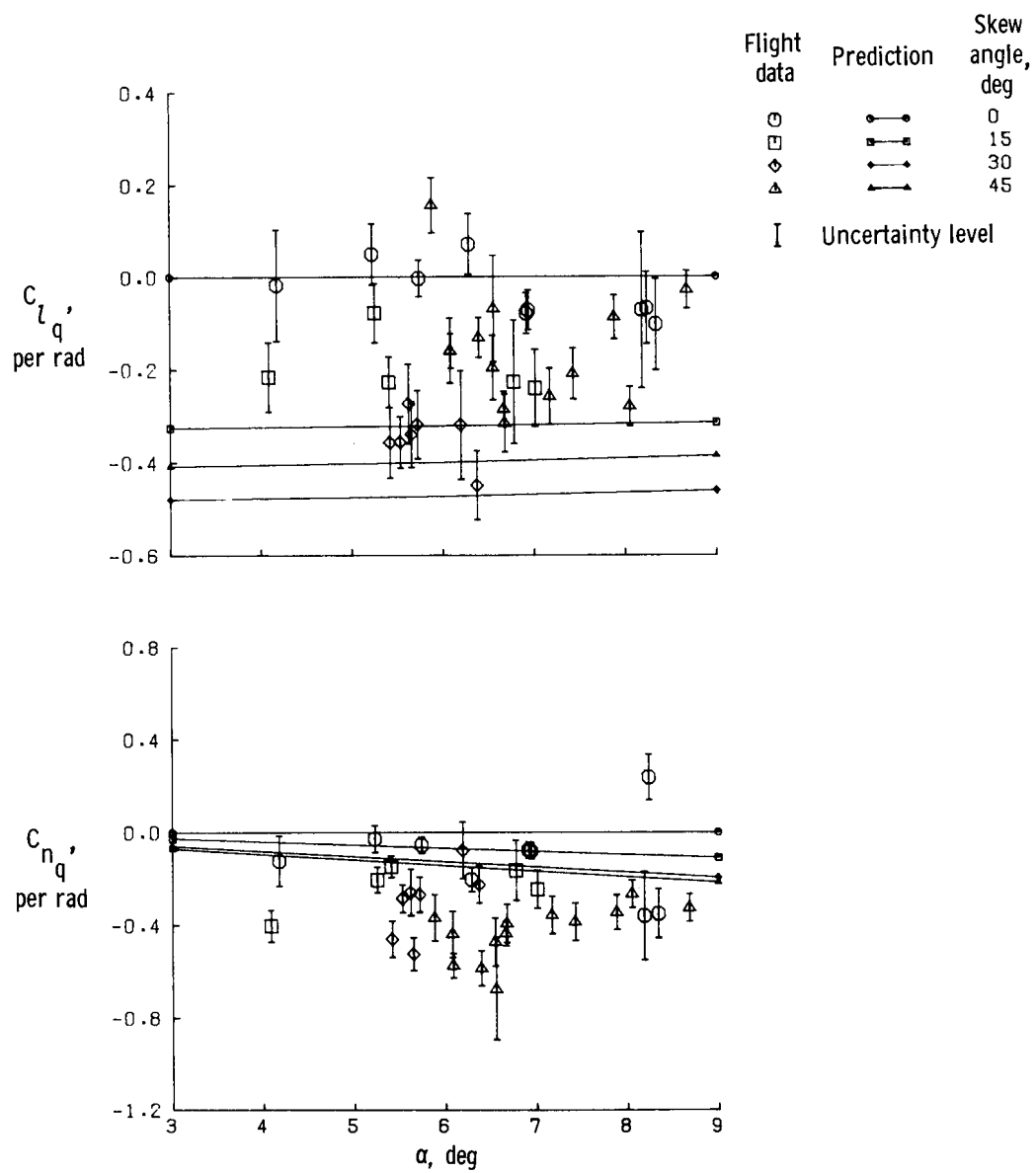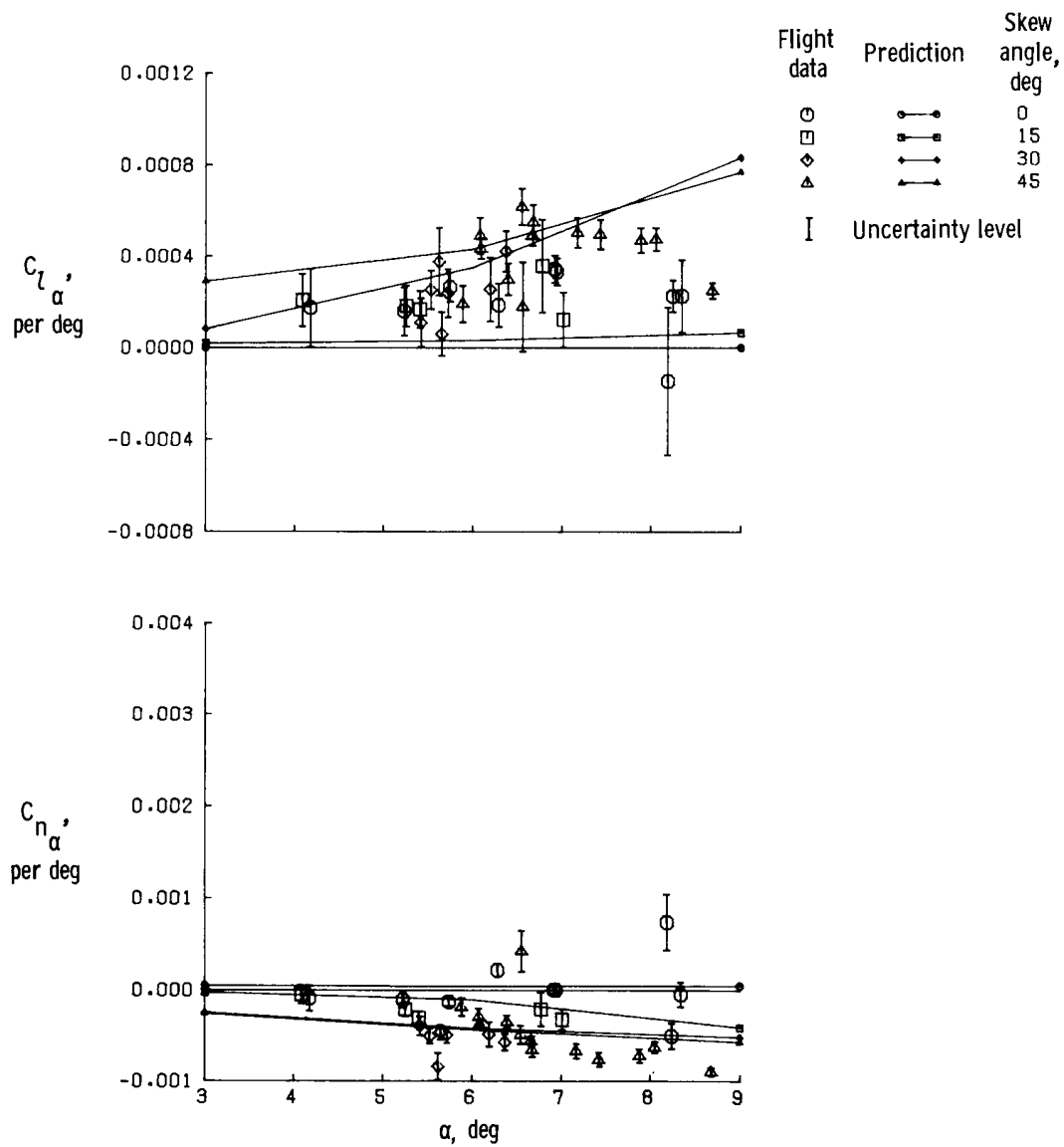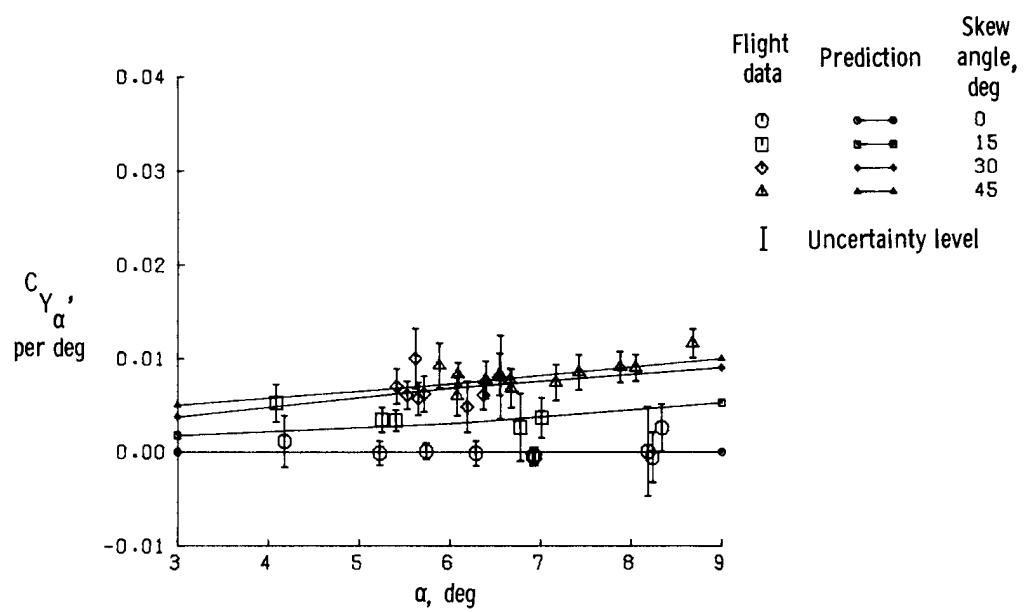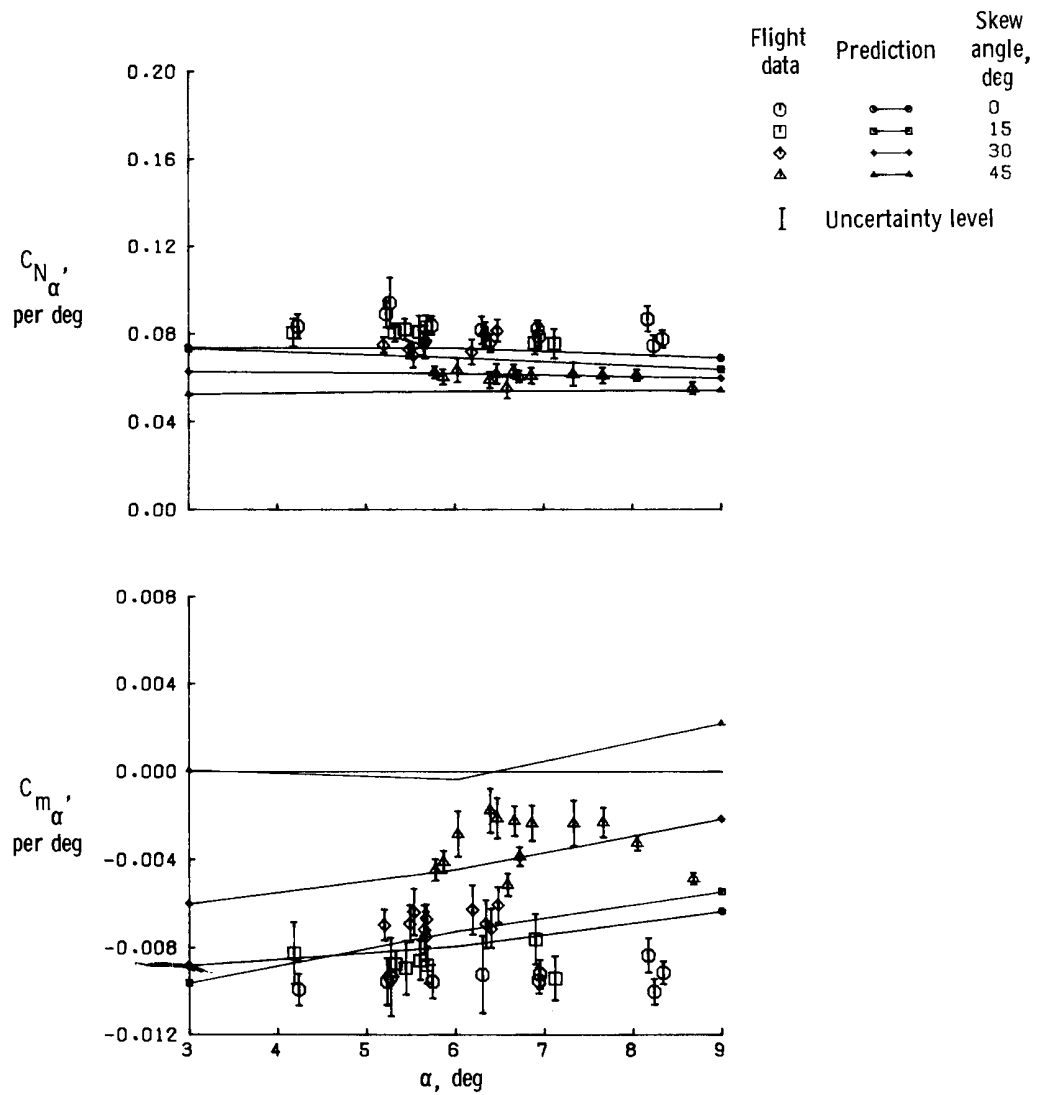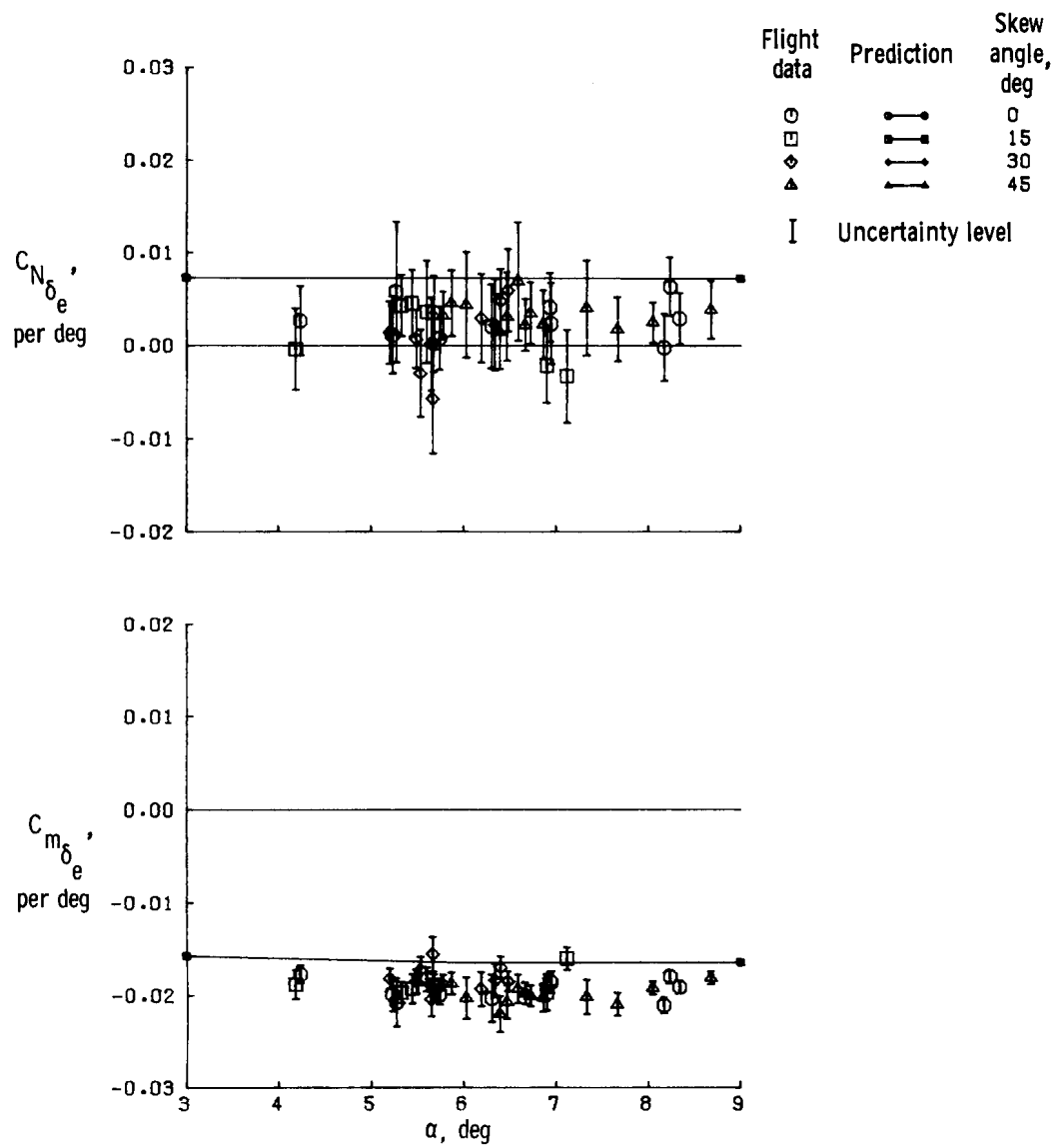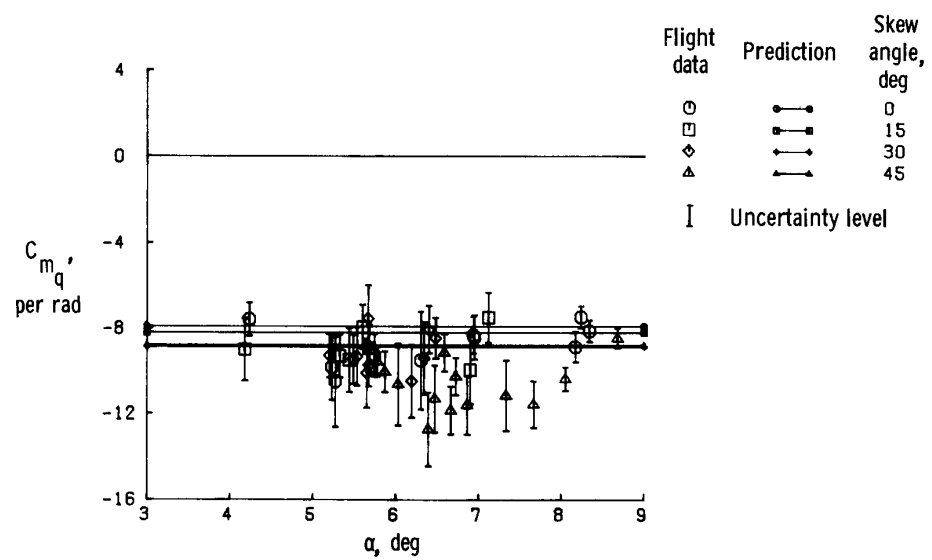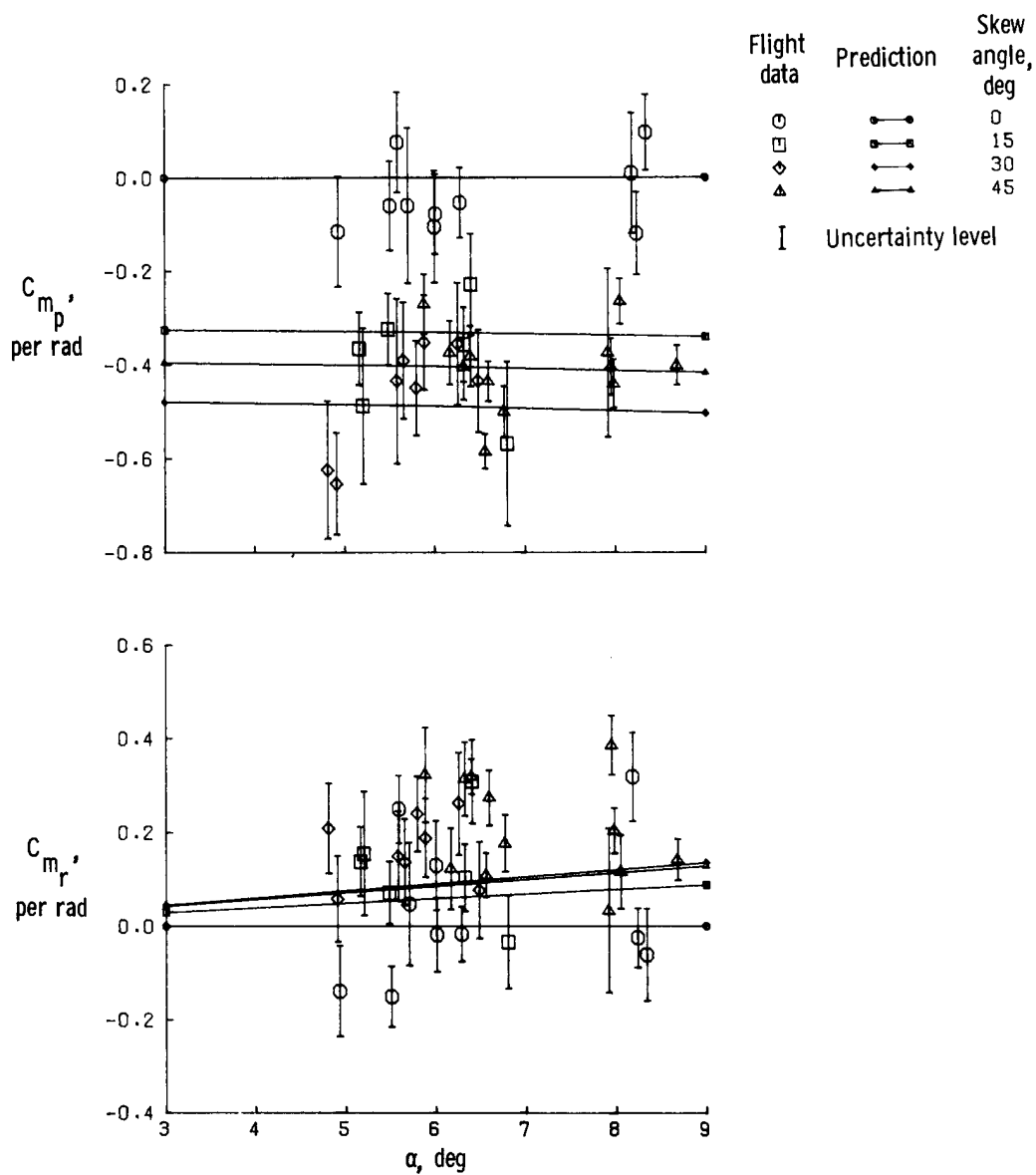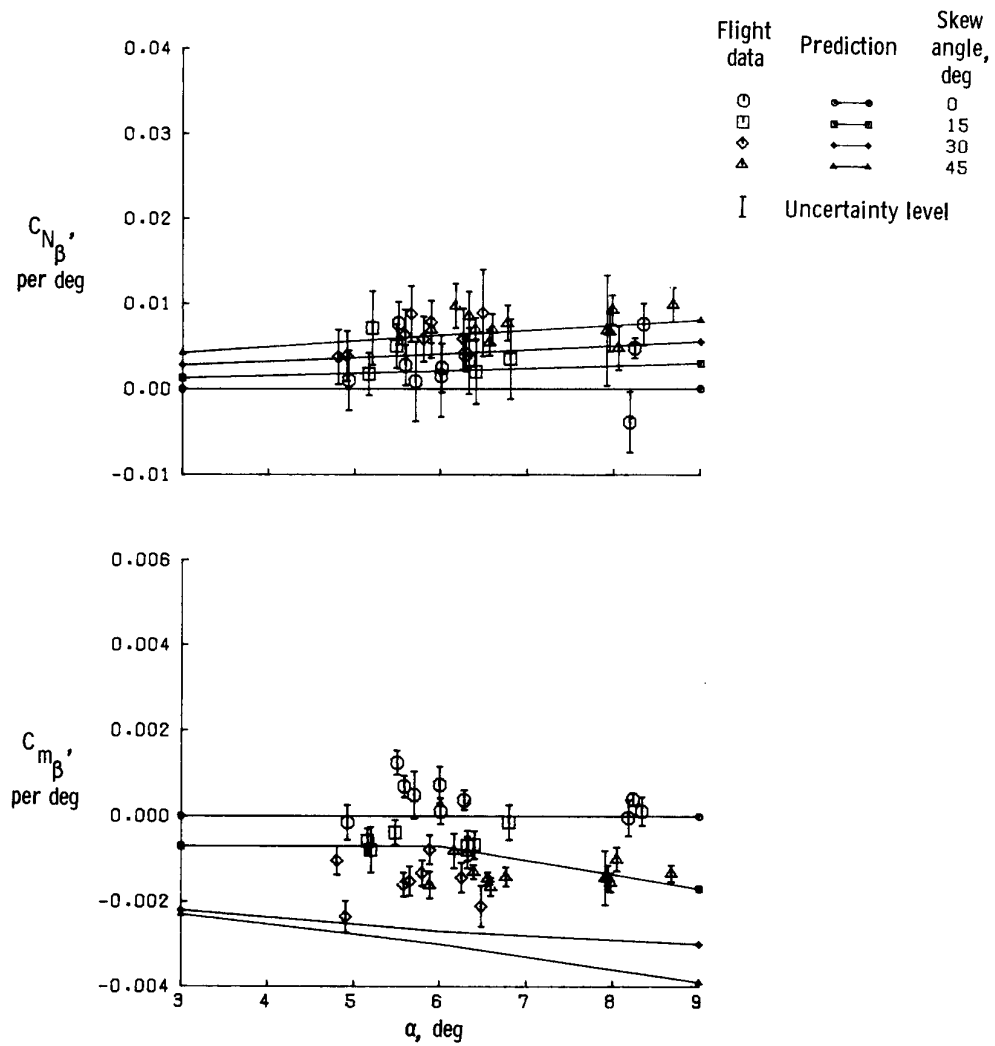*Figure 20. Longitudinal cross-coupling derivatives of oblique wing aircraft in long tail configuration.*
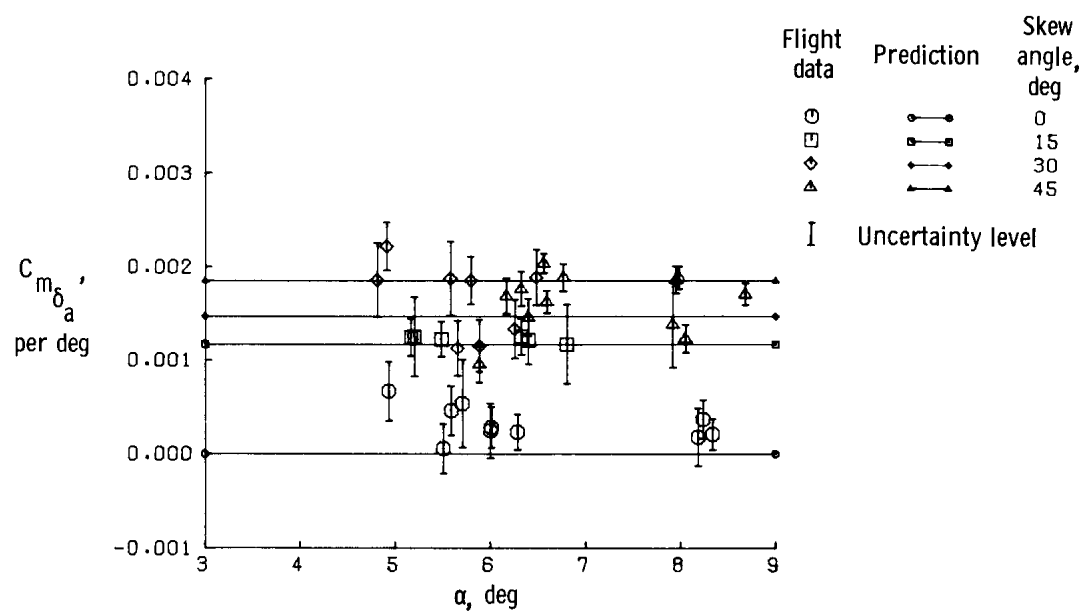
Figure 20. Continued.

Figure 20. Concluded.

1. Report No. NASA TP-1336	2. Government Accession No.	3. Recipient's Catalog No.
4. Title and Subtitle AERODYNAMIC DERIVATIVES FOR AN OBLIQUE WING AIRCRAFT ESTIMATED FROM FLIGHT DATA BY USING A MAXIMUM LIKELIHOOD TECHNIQUE		5. Report Date October 1978
		6. Performing Organization Code
7. Author(s) Richard E. Maine		8. Performing Organization Report No. H-1003
9. Performing Organization Name and Address NASA Dryden Flight Research Center P. O. Box 273 Edwards, California 93523		10. Work Unit No. 505-11-54
		11. Contract or Grant No.
12. Sponsoring Agency Name and Address National Aeronautics and Space Administration Washington, D. C. 20546		13. Type of Report and Period Covered Technical Paper
		14. Sponsoring Agency Code

15. Supplementary Notes

This report is an expansion of the material presented in AIAA Paper No. 77-1135, "Maximum Likelihood Estimation of Aerodynamic Derivatives for an Oblique Wing Aircraft From Flight Data" by the same author.

16. Abstract

There are several practical problems in using current techniques with five-degree-of-freedom equations to estimate the stability and control derivatives of oblique wing aircraft from flight data. A technique has been developed to estimate these derivatives by separating the analysis of the longitudinal and lateral-directional motion without neglecting cross-coupling effects. Although previously applied to symmetrical aircraft, this technique was not expected to be adequate for oblique wing vehicles. This report describes the application of the technique to flight data from a remotely piloted oblique wing aircraft. The aircraft instrumentation and data processing are described, with particular emphasis on the digital filtering of the data. A complete set of flight-determined stability and control derivative estimates is presented and compared with predictions. The results demonstrated that the relatively simple approach developed was adequate to obtain high quality estimates of the aerodynamic derivatives of such aircraft.

17. Key Words (Suggested by Author(s)) Oblique wing Stability and control derivatives Parameter estimation Maximum likelihood	18. Distribution Statement Unclassified - Unlimited STAR Category: 02		
19. Security Classif. (of this report) Unclassified	20. Security Classif. (of this page) Unclassified	21. No. of Pages 74	22. Price* $4.25

*For sale by the National Technical Information Service, Springfield, Virginia 22161